

# Fwd: PNAS MS# 2020-24792RR Decision Notification

---

From: **Kelly Caylor** | caylor@ucsb.edu

Monday, Aug 23, 10:35 AM

To: **Kelly Caylor** | caylor@ucsb.edu

Kelly Caylor  
Director, Earth Research Institute  
Professor  
Department of Geography  
Bren School of Environmental Science and Management  
University of California, Santa Barbara  
[caylor.eri.ucsb.edu](http://caylor.eri.ucsb.edu)

From: To: **journalstaff@pnascentral.org**

Wednesday, Jun 23, 8:48 AM

June 23, 2021

Title: "**Global Urban Population Exposure to Extreme Heat**"

Tracking #: 2020-24792RR

Authors: Tuholske et al.

Dear Dr. Tuholske,

We are pleased to inform you that the PNAS Editorial Board has given final approval of your article for publication. Matei Georgescu, the Editor who conducted the initial review of your manuscript [MS# 2020-24792RR], will also be informed of the decision.

The editorial staff may contact you shortly if final publication ready files are needed. Please note you may be asked to shorten your manuscript upon receipt of the article proof if the work does not adhere to the [stated length requirements](#) and [additional fees](#) may apply.

Within 48 hours of receipt of your proofs, you will receive an email from [PNAS](#) with a link to your publication charge estimate in our online billing platform. Please see the PNAS Author Center for information about publication fees. Authors of research articles may pay a surcharge to make their paper freely available through the PNAS Open Access option. If your institution has a current Site License, the open access surcharge is discounted. Brief Report publication fees include Open Access. Proofs should be returned within 48 hours.

Papers "in press" at PNAS are under embargo and not for public release before 3:00 PM Eastern Time, the Monday before publication. Authors may talk with the press about their work prior to the embargo but should

coordinate this with the PNAS News Office or their institution's press office so that reporters are aware of PNAS policy and understand that papers are embargoed until the week of publication. If you plan to present your embargoed paper at a conference prior to publication, please contact the PNAS News Office immediately at 202-334-1310, or [PNASnews@nas.edu](mailto:PNASnews@nas.edu).

Authors are invited to submit scientifically interesting and visually arresting cover illustrations. To view accepted cover art, please visit the [PNAS cover archive](#). Please note that images must be original and that exclusive rights to publish will convey to PNAS. If selected for the cover, the image also may be used further in promotional materials, including but not limited to brochures, advertisements, and posters. To submit cover art candidates, please send files to [PNASCovers@nas.edu](mailto:PNASCovers@nas.edu)

If you provided your ORCID iD when submitting your manuscript, you can opt in to have your ORCID record automatically updated when your article is published. You will need to watch for an email from Crossref in your ORCID Inbox requesting permission to access your ORCID record and grant Crossref permission.

Yours,  
May R. Berenbaum  
Editor-in-Chief

\*\*\*\*\*

---

# **Title: Global Urban Population Exposure to Extreme Heat**

**Authors:** Cascade Tuholske<sup>1,2,3,\*</sup>, Kelly Caylor<sup>1,4</sup>, Chris Funk<sup>1,2</sup>, Andrew Verdin<sup>5</sup>, Stuart Sweeney<sup>1</sup>, Kathryn Grace<sup>5,6</sup>, Pete Peterson<sup>2</sup>, and Tom Evans<sup>7</sup>

## **Affiliations:**

1. Department of Geography, University of California, Santa Barbara, CA, 93106 USA.
2. Climate Hazards Center, University of California, Santa Barbara, CA, 93106 USA.
3. Center for International Earth Science Information Network, The Earth Institute, Columbia University, NY 10964 USA.
4. Bren School of Environmental Science & Management, University of California, Santa Barbara, CA, 93106 USA.
5. Minnesota Population Center, University of Minnesota Twin Cities, MN, 55455 USA.
6. Department of Geography, Environment and Society, University of Minnesota Twin Cities, MN, 55455 USA.
7. School of Geography and Development, University of Arizona, AZ, 85719, USA.

\*Corresponding to: Cascade Tuholske ([cascade@ucsb.edu](mailto:cascade@ucsb.edu))

**Author contributions:** CT conceptualized the project, with intellectual contributions from all authors throughout. CT and KC wrote all project code. CT conducted all formal analysis, made figures, and wrote the original draft. AV, CF, & PP led CHIRTS-daily temperature and RH development and data curation. All authors reviewed and edited the final manuscript.

**Competing interests:** The authors declare no competing interests.

**Keywords [3-5]:** sustainability, climate change, demographics, extreme hazards, public health

## **Classification:**

1. Social Sciences (major), Environmental Sciences (minor), Sustainability Sciences (minor)
2. Physical Sciences (major), Environmental Sciences (minor), Sustainability Sciences (minor)

## **This PDF file includes:**

Main Text  
Figures 1 to 4

**Abstract:**

Increased exposure to extreme heat from both climate change and the urban heat island effect – total urban warming – threatens the sustainability of rapidly growing urban settlements worldwide. Extreme heat exposure is highly unequal, with the urban poor most severely impacted. While previous studies have quantified global exposure to extreme heat, the lack of a globally comparable, accurate, and fine-resolution temporal analysis of urban exposure crucially limits our ability to deploy adaptations. Here we estimate daily urban population exposure to extreme heat for 13,115 urban settlements from 1983 to 2016. We harmonize new global, fine-resolution ( $0.05^\circ$ ) daily temperature maxima and relative humidity estimates with the first geolocated and longitudinal global urban population database. We measure the average annual rate of increase in exposure (person-days  $\text{yr}^{-1}$ ) at the global, regional, national, and municipality-level, separating the contribution to exposure trajectories from urban population growth versus total urban warming. Using a daily maximum wet bulb globe temperature threshold of  $30^\circ\text{C}$ , global exposure increased nearly 200% from 1983 - 2016 and total urban warming elevated the annual increase in exposure by 52% compared to urban population growth alone. Exposure trajectories increased for nearly half of urban settlements, which together in 2016 comprised over a fifth of the planet's population, or 1.7 billion people. However, how total urban warming and population growth drove exposure trajectories is spatially heterogeneous. This study reinforces the importance of employing multiple extreme heat exposure metrics to identify local patterns and compare exposure trends across geographies. Our results suggest that previous research underestimates extreme heat exposure, highlighting the urgency for targeted adaptations and early warning systems to reduce harm from urban extreme heat exposure.

**Significance statement:**

Increased extreme heat exposure from both climate change and the urban heat island effect threatens rapidly growing urban settlements worldwide. Yet, because we do not know where urban population growth and extreme heat intersect, we have limited capacity to reduce the impacts of urban extreme heat exposure. Here we leverage new, fine-resolution temperature and population data to measure urban extreme heat exposure for 13,115 cities from 1983 - 2016. Globally, urban exposure increased nearly 200%, affecting 1.7 billion people. Total urban warming elevated exposure rates 52% above population growth alone. However, spatially heterogeneous exposure patterns highlight an urgent need for locally tailored adaptations and early warning systems to reduce harm from urban extreme heat exposure across the planet's diverse urban settlements.

## MAIN TEXT

### Introduction:

Increased exposure to extreme heat from both climate change (1–5) and the urban heat island (UHI) effect (6–9) threaten the sustainability of rapidly growing urban settlements worldwide. Exposure to dangerously high temperatures endangers urban health and development, driving reductions in labor productivity and economic output (10, 11) and increases in morbidity (1) and mortality (3, 4, 12). Within urban settlements, extreme heat exposure is highly unequal and most severely impacts the urban poor (13, 14). Despite the harmful and inequitable risks, we presently lack a globally comprehensive, fine-resolution understanding of where urban population growth intersects with increases in extreme heat (3, 6, 15). Without this knowledge, we have limited ability to tailor adaptations to reduce extreme heat exposure across the planet’s diverse urban settlements (6, 15, 16).

Reducing the impacts of extreme heat exposure to urban populations requires globally consistent, accurate, and high-resolution measurement of both climate and demographic conditions that drive exposure (2, 15, 17). Such analysis provides decision makers with information to develop locally-tailored interventions (7, 18, 19) and is also sufficiently broad in spatial coverage to transfer knowledge across urban geographies and climates (6). Information about exposures and interventions from diverse contexts is vital for the development of functional early warning systems (20) and can help guide risk assessments and inform future

scenario planning (21). Existing global extreme heat exposure assessments (1, 3), however, do not meet these criteria (Table S1) and are insufficient for decision makers. These studies are coarse-grained ( $>0.5^\circ$  spatial resolution), employ disparate or single metrics that do not capture the complexities of heat-health outcomes (22), do not separate urban from rural exposure (19), and rely on climate reanalysis products that can be substantially ( $\sim 1$  to  $3^\circ\text{C}$ ) cooler than in-situ data observations (2, 23, 24). In fact, widely-cited benchmarks (25) that estimate extreme heat with the version 5 of the European Centre for Medium-Range Weather Forecasts Reanalysis (ERA5) (26) may greatly underestimate total global exposure to extreme heat (2, 23, 24). Using a  $40.6^\circ\text{C}$  daily maximum 2m air temperature threshold ( $T_{\text{max}}$ ), recent analysis found that ERA5  $T_{\text{max}}$  drastically underestimated the number of extreme heat days per year compared to in-situ observations (23). Finally, few studies (3, 18) have assessed urban extreme heat exposure across data-sparse (23) rapidly urbanizing regions, such as Sub-Saharan Africa, the Middle East, and Southern Asia (27), that may be most impacted by increased extreme heat events due to climate change (2, 4, 28).

Here we present the first globally comprehensive, fine-resolution, and longitudinal estimate of urban population exposure to extreme heat—referred to henceforth as *exposure*—for 13,115 urban settlements from 1983 to 2016. To accomplish this, we harmonize new global, fine-grained ( $0.05^\circ$  spatial resolution)  $T_{\text{max}}$  estimates (23) with new global urban population and spatial extent data (29). For each urban settlement, we calculate area-averaged daily maximum wet bulb globe temperature ( $\text{WBGT}_{\text{max}}$ ) (30) and heat index maxima  $\text{HI}_{\text{max}}$  (31) using CHIRTS-daily  $T_{\text{max}}$  (23) and down-scaled daily minimum relative humidity ( $\text{RH}_{\text{min}}$ ) estimates (32). CHIRTS-daily is better suited to measure urban extreme heat exposure than other gridded

temperature datasets used in recent global extreme heat studies (Table S1) for two reasons. First, it is more accurate, especially at long distances (See Fig. 3 in (23)), than widely-used gridded temperature datasets to estimate urban temperature signals worldwide (Fig. S1-S2). Second, it better captures the spatial heterogeneity of  $T_{\max}$  across diverse urban contexts (Fig. S3). These factors are key for measuring extreme heat exposure in rapidly urbanizing, data-sparse regions.

As discussed in (23, 24), the number of in situ temperature observations is far too low across rapidly-urbanizing (27) regions to resolve spatial and temporal urban extreme heat fluctuations, which can vary dramatically over small distances and time periods. For example, of the more than 3,000 urban settlements in India (29), only 111 have reliable station observations (Fig. S3). While climate reanalyses can help overcome these limitations, they are coarse-grained (Table S1), suffer from mean bias, and, to a lesser degree, temporal fidelity. ERA5 has been shown to substantially underestimate the increasing frequencies of heat extremes (Fig. 4 in (23)), while Modern-Era Retrospective analysis for Research and Applications, Version 2 (MERRA2) fails to represent the substantial increase in recent monthly  $T_{\max}$  values (Fig. 8 in (24)). These datasets dramatically underestimate increases in warming. CHIRTS-daily overcomes these limitations by coherently stacking information from a high-resolution climatology ( $0.05^\circ$ ), derived surface emission temperatures (24), interpolated in situ observations, and ERA5 reanalysis to produce a product that has been explicitly developed to monitor and assess temperature related hazards (23). As such, CHIRTS-daily is best suited to capture variation in exposure across urban settlements in rapidly urbanizing (27), data-sparse regions such as Sub-Saharan Africa, the Middle East, and Southern Asia (Fig. S3) (24).

We measure exposure in person-days  $\text{yr}^{-1}$  – the number of days per year that exceed a heat exposure threshold multiplied by the total urban population exposed (2). We then estimate annual rates of increase in exposure at the global (Fig. 1), regional (Table S2), national (Table S3), and municipality levels from 1983 - 2016 (Table S4). At each spatial scale, we separate the contribution to exposure trajectories from total urban warming and population growth (2). For clarity, *total urban warming* refers to the combined increase of extreme heat in urban settlements from both the UHI effect and anthropogenic climate change. We do not decouple these two forcing agents (33, 34). However, we identify which urban settlements have warmed the fastest by measuring the rate of increase in the number of days per year that exceed the two extreme heat thresholds described below (15). Our main findings use an extreme heat exposure threshold defined as  $\text{WBGT}_{\text{max}} > 30^{\circ}\text{C}$ , the International Standards Organization (ISO) occupational heat stress threshold for risk of heat-related illness among acclimated persons at low metabolic rates (100-115W) (30).  $\text{WBGT}_{\text{max}}$  is a widely used heat stress metric (36) that captures the biophysical response (35) of hot temperature-humidity combinations (4, 17) that reduce labor output (35), lead to heat related illness (35) and can cause death (23). In using a threshold  $\text{WBGT}_{\text{max}} > 30^{\circ}\text{C}$ , which has been associated with higher mortality rates among vulnerable populations (37), we aim to identify truly extremely hot temperature-humidity combinations (17) that can harm human health and wellbeing. We recognize, however, that strict exposure thresholds do not account for individual-level risks and vulnerabilities related to acclimatization, socio-economic or health status or local infrastructure (18, 19, 38). We also note that there are a range of definitions of exposure and we provide further analysis identifying 2-day or longer periods where the



maximum heat index ( $HI_{\max}$ ) (31) exceeded  $40.6^{\circ}\text{C}$  (Fig. S4-S6) following the US National Weather Service's definition for an excessive heat warning (39).

## **Results and Discussion:**

Global exposure increased 199% in 34-years, from 40 billion person-days in 1983 to 119 billion person-days in 2016, growing by 2.1 billion person-days  $\text{yr}^{-1}$  (Fig. 1A). Population growth (Fig. 1B) and total urban warming (Fig. 1C) contributed 66% (1.5 billion person-days  $\text{yr}^{-1}$ ) and 34% (0.7 billion person-days  $\text{yr}^{-1}$ ) to the annual rate of increase in exposure, respectively. That is, total urban warming elevated the global annual rate of increase in exposure by 52% compared to urban population growth alone. This finding is not directly comparable to recent global benchmarks and projections of total population exposure to extreme heat because of disparate exposure definitions employed (Table S1). However, our results indicate much higher exposure rates compared to recent continental-scale benchmarks. Defining exposure as the total population multiplied by the number of days per year where  $HI_{\max} > 40.6^{\circ}\text{C}$ , a recent study found that the total annual average exposure from 1986 - 2005 for 173 African cities was 4.2 billion person-days  $\text{yr}^{-1}$  (40). When we apply the same exposure criteria to our data, including parameterizing  $HI_{\max}$  with daily average RH instead of  $RH_{\min}$ , we find six times the average total exposure for Africa, or 27.5 billion person-days  $\text{yr}^{-1}$ , over the same time period. This contrasting exposure estimate showcases how the increased spatial and temporal accuracy of CHIRTS-daily  $T_{\max}$  (Fig. S1-S3), combined with the increased granularity of urban settlement data we employ (29), can better capture exposure trends in data-sparse regions like Africa.

While just 25 urban settlements contributed nearly 25% of the global annual rate of increase in exposure (Table S3), we identify statistically significant ( $p < 0.05$ ) positive exposure

trajectories from 1983 - 2016 for nearly half (5,985) of municipalities worldwide (Fig 2A). Together, these urban settlements comprised 23% of the planet's total population (27), or 1.7 billion people, in 2016 (27). The majority are concentrated in low-latitudes but span a range of climates. Additionally, 17% (2,252) of urban settlements added at least one day per year where  $WBGT_{max}$  exceeded  $30^{\circ}C$  (Fig. 2B). In other words, these urban settlements experienced an additional month of extreme heat in 2016 compared to 1983. Remarkably, 21 urban settlements with populations greater than 1 million residents in 2016 added more than 1.5 days per year of extreme heat. This includes Kolkata, India, which is the capital of the state of West Bengal and housed 22 million people in 2016 (29). These findings suggest that increased extreme heat is potentially elevating mortality rates for many of the planet's urban settlements, especially among those most socially and economically marginalized (37). Globally, for every additional day  $T_{max}$  exceeds  $35^{\circ}C$  compared to  $20^{\circ}C$ , mortality increases by 0.45 per 100,000 people, with an increase of 4.7 extra deaths per 100,000 people for those above 64 years old (12).

Separating the contribution to exposure trajectories from urban population growth and total urban warming underscores how the level of analysis affects our understanding of the spatial distribution and magnitude of exposure. The level of analysis employed can either mask or highlight spatial and temporal patterns that are key to allocating limited resources for adaptations and sharing knowledge across urban contexts (2, 3, 6, 7). Broadly, we find that municipality-level exposure trajectories (Fig. 2C) reflect national and regional-level urbanization trends (27). In regions with slower urban population growth (27), like Latin America and the Caribbean (Fig. 3A) (27), the contribution of total urban warming to increases in exposure trajectories compared to urban population growth is largely responsible for increased exposure

for the majority of municipalities compared to regions with more rapid urban population growth. As urban population growth rates increase by region, the signal from total urban warming diminishes for most municipalities, as evident by Western Asia (Fig. 3B), Southern Asia (Fig. 3C), and sub-Saharan Africa (Fig 3D).

However, we detail striking spatial heterogeneity in how urban demographic and total urban warming signals drive exposure trajectories for individual municipalities, even those with similar population sizes and within the same country. As such, regional and national-level assessments designed to inform policy implementation (1, 41), may fail to capture municipality-level (and finer scale) nuances that are key for adaptations (7, 15) and future climate change scenario planning (21) (Supplementary Text, Fig. S7-S8). For example, in West Africa, while we find exposure trajectories increased for 88% of Nigerian urban settlements, the disparate influence of total urban warming across urban settlements may be dictated by local climate (Supplementary Text, Fig. S8). Furthermore, we map pockets of urban settlements in Southern India, the Ganges Delta, the Nile river valley and delta, and along the Tigris-Euphrates (Fig. 2C, Fig. S9)—all rapidly urbanizing regions (1)—where total urban warming exceeded urban population growth as the driver of exposure. This geographic pattern parallels recent global analysis of station observations of extreme humid heat that suggest areas of the planet may soon exceed human biophysical capacity, regardless of local acclimatization (17).

Among the clearest examples of the importance of differentiating urban demographic and total urban warming signals at the municipality-level comes from two Indian megacities: Delhi and Kolkata. Exposure trajectories for both cities are congruent (Table 3, Fig. S10A). But population growth contributed to nearly 75% of the increase in Delhi's exposure trajectory,

whereas population growth accounted for only 48% of the annual rate of increase in exposure in Kolkata (Table S4, Fig. S10B-C). The stark contrast in the impact of total urban warming versus urban population growth on the two cities' exposure trajectories (Fig. S10) reinforces that individual adaptations require fine-grained spatiotemporal, yet globally comparable, analysis (6, 15). Such precision is crucial for decision makers given the range of adaptation choices and costs (7, 15), and also opens new avenues of inquiry to examine linkages between elevated temperatures, changes in humidity, and drivers of urban population growth (16, 42–45).

Finally, while our main findings focus on exposure determined by  $WBGT_{max} > 30^{\circ}C$ , we showcase the contrast between  $WBGT_{max}$  and  $HI_{max}$  exposure estimates with two examples of poorly documented local urban extreme heat events. First, air temperatures that reached  $49.8^{\circ}C$  reportedly killed thousands of people in India in 1998 (46). But the reports do not specify nor identify impacts specific to urban settlements. In Kolkata, which was home to 12 million people in 1998 (27), we find that  $HI_{max}$  exceeded  $40.6^{\circ}C$  for 53 consecutive days in May - June 1998 (Fig. 4A). During this period the average  $HI_{max}$  exceeded the 34-year daily  $HI_{max}$  average by as much as  $9^{\circ}C$ . (27). The amplitude of daily extreme temperature-humidity combinations however, is not resolved using  $WBGT_{max}$  (Fig. 4B) because  $WBGT_{max}$  saturates at high values (47).

Next, we examine the summer of 2010 in Syria, which was the final year of a 4-year drought that was 2 to 3 times more likely because of climate change (48). In Aleppo, home to 3 million people in 2010 (27), we document an 8-day period shortly followed by a 7-day period with  $HI_{max}$  above  $40.6^{\circ}C$  (Fig. 4C). We isolate the peak of the heat wave hitting Aleppo on Aug. 5, during which  $HI_{max}$  exceeded  $47^{\circ}C$  ( $9^{\circ}C$  above average  $HI_{max}$  for Aug. 5) and marked the second hottest day in the entire 34-year record. Yet, like Kolkata in 1998, the amplitude of the

extreme heat events in Aleppo in 2010 is not captured by  $WBGT_{max}$  compared to  $HI_{max}$  (Fig. 4D). While the likelihood of heat waves has increased for the Eastern Mediterranean since the 1960s (49), to our knowledge, urban extreme heat during the summer of 2010 in Syria has not been documented nor quantified until now. This extreme heat event occurred six months prior to the beginning of the Syrian uprising. While conflict and climate linkages are inconclusive and complex (50, 51), this finding from Aleppo illustrates potential advantages of higher-resolution data and analysis we present here for future research to examine climate-conflict linkages.

We present these examples not to advocate for or against the use of either  $WBGT_{max}$  or  $HI_{max}$  to measure exposure. Both have limitations when independently used to quantify extreme heat exposure.  $HI_{max}$  was not intended to estimate heat exposure above  $HI_{max} \sim 50^{\circ}\text{C}$  (52) and the quadratic relationship we used to convert  $HI_{max}$  to  $WBGT_{max}$  explains the asymptotic ceiling of  $WBGT_{max}$  and its failure to capture daily extremes like  $HI_{max}$  does (47). Rather we join the growing community of scholars advocating for the use of multiple (22), place-based heat wave metrics that inform and create better synergies across research domains (19). Locally-defined exposure criteria (18) are especially useful for early warning systems (53) when tied to biophysical response of extreme heat with impacts on individual-level human health and wellbeing (19, 22), as well as be comparable across geographies (6).

By focusing on extremely hot-humid exposure defined by (6)  $>30^{\circ}\text{C}$ , our global synthesis of urban extreme heat exposure is conservative. For example, when we adjust the threshold to (6)  $WBGT_{max} > 28^{\circ}\text{C}$  (Fig. S11), the ISO occupational standard risk for heat-related illness for acclimated people at moderate metabolic rates (235-360W) (30), 7,628 urban settlements have a significant ( $p < 0.05$ ) in exposure from 1983 - 2016 (Fig. S11). In contrast, when we adjust the

threshold to  $WBGT_{max} > 32^{\circ}C$ , the ISO heat-risk threshold for unacclimated people at resting metabolic rates (100-125W) (30), 2,979 urban settlements have a significant ( $p < 0.05$ ) increase in exposure from 1983 – 2016 (Fig. S11). Accordingly, our findings suggest that in already hot regions, like the Sun Belt Region in the United States, where air temperatures are projected to increase (18), temperature-humidity (6) combinations may not regularly exceed extremes like  $WBGT_{max} > 32^{\circ}C$  for many urban settlements. For example, take Phoenix, Arizona. The hottest  $T_{max}$  ever recorded in Phoenix was  $122^{\circ}F$  on June 26, 1990 at 23h GMT (54, 55). The relative humidity at that time was 11% (54). Following our methods, the  $HI_{max}$  equivalent was  $49^{\circ}C$  and the equivalent  $WBGT_{max}$  was  $32.29^{\circ}C$ . Thus, vulnerable population regularly experience extreme heat exposure in Phoenix (56, 57), demonstrating the need for diverse definitions of heat stress.

In sum, our analysis calls into question the future sustainability and equity for populations living in and moving to many of the planet's urban settlements. Climate change is increasing the frequency, duration, and intensity of extreme heat across the globe (1–5). Indeed, combined temperature and humidity extremes already exceed human biophysical tolerance in some locations (17). Poverty reduction in urban settlements ultimately hinges on increasing labor productivity (10) but, across spatial scales, elevated temperatures have been associated with decreased economic output (11, 58, 59). As such, the spatial pattern of exposure trajectories we identify in Africa and Southern Asia, which already house hundreds of millions of the urban poor (60), highlight that, without sufficient investment, humanitarian intervention, and government support, extreme heat may crucially limit the urban poor's ability to realize the economic gains associated with urbanization (61). Synthesizing extreme heat exposure across all individual urban settlements globally, however, reveals that exposure trajectories are composed of

thousands of extreme heat events. Each of those events presents an opportunity for effective early warning, a tool that, if widely implemented, can reduce the burden extreme heat places on all urban populations (20).

## **Materials and Methods:**

### **Daily Temperature**

The new Climate Hazards Center InfraRed Temperature with Stations Daily (CHIRTS-daily) provides globally extensive, high-resolution ( $0.05^\circ$ ) daily maximum and minimum temperature estimates ( $T_{\max}$  and  $T_{\min}$ ) from 1983 – 2016 (23). CHIRTS-daily  $T_{\max}$  and  $T_{\min}$  are produced by bias correcting ERA5  $T_{\max}$  data with the monthly averaged  $T_{\max}$  from the Climate Hazards center InfraRed Temperature with Stations (CHIRTS<sub>max</sub>) climate data record (24). By combining cloud-screened harmonized geostationary satellite thermal infrared (TIR) observations with approximately 15,000 in-situ station observations from Berkeley Earth (62), CHIRTS<sub>max</sub> is the most accurate ( $R^2 = 0.8 - 0.9$ ) high-resolution monthly maximum temperature datasets with global coverage (24). The advantage of CHIRTS<sub>max</sub> is that it captures  $T_{\max}$  in rapidly urbanizing (27), yet data sparse regions (Fig. S1-S2). Indeed, from 1983 to 2016, station-based daily observations of temperature maxima declined globally from 5,900 to 1,000 (24). This decline was especially acute in Sub-Saharan Africa, the Middle East and Southern Asia, regions that have the fastest growing urban populations (27). Validation of CHIRTS-daily  $T_{\max}$  against Global Historical Climatology Network and Global Summary of the Day databases show that CHIRTS-daily consistently outperforms the widely used Princeton University's Global Meteorological Forcing Dataset (PGF) for land surface modeling (Figs. S1-3) (63) as well ERA5 (26).

The methodology used to produce the CHIRTS-daily  $T_{\max}$  relies on fusing the skill of CHIRTS<sub>max</sub> at measuring high-spatial resolution monthly climatology (24) with the ability of ERA5  $T_{\max}$  to measure daily temperature anomalies. To produce CHIRTS-daily  $T_{\max}$ , first, ERA5  $T_{\max}$  and  $T_{\min}$  are down-scaled from 0.25° latitude by 0.25° longitude to 0.05° by 0.05° using bilinear interpolation to match the spatial resolution of CHIRTS<sub>max</sub>. Next, the ERA5 daily diurnal temperature range (DTR) is calculated by subtracting ERA5 daily  $T_{\max}$  from ERA5 daily  $T_{\min}$  (DTR) (eq. 1). ERA5 daily  $T_{\max}$  are then converted to anomalies, by subtracting the ERA5 monthly  $T_{\max}$  average from the daily ERA5  $T_{\max}$  value (eq. 2). The ERA5  $T_{\max}$  daily anomalies are then added to the CHIRTS<sub>max</sub> value for a given month (eq. 3). CHIRTS-daily  $T_{\min}$  is produced by subtracting the ERA5 daily diurnal temperature (DTR) from CHIRTS-daily  $T_{\max}$  (eq. 4). This process is repeated across all months and all days from 1983 - 2016 and can be expressed as

$$DTR_t = ERA5 T_{max_t} - ERA5 T_{min_t} \text{ for } t = 1 \dots T \text{ (eq. 1)}$$

$$ERA5 T_{max_t}^{m, anomn} = ERA5 T_{max_t}^t - ERA5 T_{max}^m \text{ for } t = 1 \dots T, m = 1 \dots M \text{ (eq. 2)}$$

$$CHIRTS_{daily} T_{max} = CHIRTS_{max} + ERA5 T_{max_t}^{m, anomn} \text{ (eq. 3)}$$

$$CHIRTS_{daily} T_{min} = CHIRTS_{daily} T_{max} - DTR_t \text{ (eq. 4)}$$

where  $T$  is all the days ( $t$ ) in the CHIRTS-daily record and  $M$  is all the months ( $m$ ) in the CHIRTS<sub>max</sub> record from 1983 – 2016.

### **Daily Relative Humidity Product**



Because  $T_{\max}$  generally occurs when RH is lowest during a diurnal cycle (32), daily relative humidity minimum fields ( $RH_{\min}$ ) are calculated (Eq. 5-7) by combining CHIRTS-daily  $T_{\max}$  with downscaled ERA5 dew-point pressure ( $T_d$ ) and surface pressure ( $p$ , kg / kg) from Modern-Era Retrospective analysis for Research and Applications, Version 2 (MERRA-2). ERA5  $T_d$  is downscaled from  $0.25^\circ$  longitude by  $0.25^\circ$  latitude and MERRA-2  $p$  is downscaled from  $0.5^\circ$  latitude x  $0.625^\circ$  longitude to CHIRTS-daily's  $0.05^\circ$  by  $0.05^\circ$  spatial resolution using bilinear interpolation. To calculate  $RH_{\min}$  (64), first we calculated specific humidity ( $q$ ) as:

$$q = (0.622 \times e) \div (p - (0.378 \times e)) \text{ (Eq. 5)}$$

where vapor pressure in millibars ( $e$ ), is:

$$e = 6.112 \times \exp((17.67 \times T_d) \div (T_d + 243.5)) \text{ (Eq. 6)}$$

Daily  $RH_{\min}$  is then calculated, as:

$$RH_{\min} = 0.263 \times p \times q \div (\exp((17.67(T - T_0) \div T - 29.65))) \text{ (eq. 7)}$$

where  $T$  is the CHIRTS-daily  $T_{\max}$  and  $T_0$  is 273.15 to convert Kelvin to Celsius. The result is a fine-grain daily RH estimate for the entire planet from 1983 - 2016.

## Population Data

We use population estimates and spatial boundaries for 13,115 urban settlements from the Global Human Settlement Layer Urban Centers Database (GHS-UCDB) released by the European Commission Joint Research Council in 2019 (29). Available as vector shapefiles, GHS-UCDB is derived from a gridded population modeling framework that apportions finest-available census data to grid cells based on built environment detected in the Landsat archive (for a complete description see ((29)). GHS-UCDB populations are benchmarked for 1975, 1990,

2000 and 2015. To estimate populations for each GHS-UCDB polygon for each year from 1983 - 2016, we apply a stepwise linear interpolation to the 1975, 1990, 2000, and 2015 GHS-UCDB population estimates for each urban settlement.

GHS-UCDB is the only well-documented global, geo-located urban population and extent dataset. We recognize that strict definitions of urban populations often fail to capture the urban-rural continuum (65), nor the wide diversity and variation within and between urban settlements across the planet (66). But by using a uniform criterion to identify populations and boundaries of urban settlements across the planet, the GHS-UCDB allows for direct comparison of urban settlements populations across disparate geographies and maps the diverse urban settlement patterns to strict fine-grained geographic boundaries requisite to calculating urban population exposure to extreme heat globally.

### **Data Harmonization**

We convert the GHS-UCDB polygons to a raster in the same coordinate reference system (WGS 84) and spatial resolution as CHIRTS-daily  $T_{\max}$  ( $0.05^\circ$  by  $0.05^\circ$ ). We then calculate  $HI_{\max}$  and  $WBGT_{\max}$  with CHIRTS-daily  $T_{\max}$  and  $RH_{\min}$  for  $0.05^\circ$  pixels within each urban settlement from 1983 – 2016 as described below. For each urban settlement, we then area-average  $HI_{\max}$  and  $WBGT_{\max}$  for each day in the data record. We recognize the limitations of using an area-average to characterize  $WBGT_{\max}$  and  $HI_{\max}$  for an entire urban settlement, especially for large agglomerations that can span multiple climatic zones (6). However, robust global and continental-scale urban heat studies report a single temperature for urban settlements (3, 4, 6). We also note that CHIRTS-daily is available at a finer spatial resolution (Table S1) and has better

spatial and temporal fidelity, than the temperature datasets used in recent global retrospective and predictive extreme temperature studies (3, 4) and UHI effect studies (6).

### Daily Urban Heat Index Maximum Estimates

We calculate daily maximum heat index values ( $HI_{max}$ ) for  $0.05^\circ$  pixels within each urban settlement following the National Ocean and Atmospheric Administration's (NOAA) guidelines (31). First, CHIRTS-daily  $T_{max}$  (referred to as  $T_{max}$  in eq. 8 - 11 for simplicity) and  $RH_{min}$  values are transformed from Celsius to Fahrenheit. Next, daily  $HI_{max}$  values are calculated using Steadman's equation and averaged with the  $T_{max}$  value (eq. 8):

$$HI_{max} = \frac{(0.5 \times (T_{max} + 61.0 + ((T_{max} - 68.0) \times 1.2) + (0.094RH_{min})) + T_{max}}{2}$$

(eq. 8)

If the resulting averaged value is greater than 80 F, then we calculate  $HI_{max}$  for each city following the complete Rothfus equation (eq. 9):

$$HI_{max} = -42.379 + 2.04901523T_{max} + 10.14333127RH_{min} - 0.22475541T_{max}RH_{min} - .00683783T_{max}^2 - 0.05481717RH_{min}^2 + 0.00122874T_{max}^2RH_{min} + 0.00085282T_{max}RH^2 - 0.00000199T_{max}^2RH_{min}^2$$

(eq. 9)

We then adjust the Rothfus heat index values per NOAA's guidelines. For a given urban settlement on a given day, if  $T_{max}$  is between 80 and 112 °F and  $RH_{min} < 13\%$ , we subtract adjustment 1 from  $HI_{max}$  (eq. 10). If  $T_{max}$  is between 80 and 87 °F and  $RH_{min} > 85\%$ , we add adjustment 2 to  $HI_{max}$  (eq. 11). We then convert all resulting maximum daily heat index values back to Celsius.

$$ADJ1 = \frac{0.25 \times (13 - RH_{min}) \times \sqrt{(17 - ABS(T_{max} - 95))}}{17} \quad (\text{eq. 10})$$

$$ADJ2 = \frac{RH_{min} - 85}{10} \times \frac{87 - T_{max}}{5} \quad (\text{eq. 11})$$

### Daily Urban Wet Bulb Globe Temperature Maximum Estimates

Pairwise  $HI_{max}$  and  $WBGT_{max}$  values fit a quadratic relationship, with  $HI_{max}$  estimates above  $40.6^{\circ}\text{C}$  within  $\pm 0.5^{\circ}\text{C}$  of  $WBGT_{max}$  (47), a more complex measure of extreme heat that incorporates radiant heat and air speeds and is widely used to measure occupational limits to heat stress (47). As such, we convert  $HI_{max}$  pixels estimates to  $WBGT_{max}$  using eq. 12:

$$WBGT (^{\circ}\text{C}) = -0.0034 HI^2 (^{\circ}\text{F}) + 0.96 HI (^{\circ}\text{F}) - 34 \quad (\text{eq. 12})$$

### Urban Population Exposure to Extreme Heat

We identify urban extreme heat events for two criteria: one day or longer periods where  $WBGT_{max} > 30^{\circ}\text{C}$  and two day or longer periods the maximum  $HI_{max} > 40.6^{\circ}\text{C}$ . The  $WBGT_{max}$  threshold we employ follows the International Standards Organization (ISO) occupational heat stress criteria for risk of heat-related illness among acclimated people with low metabolic rates (125 - 180W) (30, 35). The  $HI_{max}$  threshold follows the US National Weather Service's definition for an excessive heat warning (39). We acknowledge that the diversity of heat wave and extreme heat event definitions reflects the wide range of disciplines studying extreme heat (22). Climate scientists tend to use strict thresholds for comparable statistics across the planet, physiologists and occupational health researchers tend to use thresholds tied to local adaptations connected to universal biophysical responses to heat stress (35). Rather than use percentile based criteria to identify heat stress that fit local contexts (18), we employ  $WBGT_{max}$  and  $HI_{max}$  thresholds for two

primary reasons: (1) to provide consistent estimates of urban heat extreme heat exposure trajectories that can be directly compared across urban geographic and spatial scales, and (2) to capture the contribution to exposure trajectories from both urban population growth and total urban warming using thresholds that have been shown to impact human health and well-being.

Furthermore, unlike extreme heat studies that solely employ 2m air temperature (1), both  $WBGT_{max}$  and  $HI_{max}$  account for the nonlinear biophysical response to the relationship between humidity and air temperature (3). Core body temperatures are almost universally maintained around 37°C and skin temperatures around 35°C (67). Hyperthermia, elevated core body temperature, occurs when elevated skin temperatures are sustained, which can result in death when core body temperatures reach around 42-43°C (68). While acclimatization can reduce the burden of heat (67, 69), acclimatization only improves sweating mechanisms, and the cooling effects of acclimated people have limits. As relative humidity increases, the evaporative cooling effects of sweating decreases and once relative humidity reaches 100%, sweating continues but evaporative cooling stops. Even acclimated or healthy humans face mortality with prolonged skin temperatures of 37–38°C (70, 71). Thus, it is reasonable that sustained periods of time with  $HI > 35^{\circ}C$  (72) can be physically intolerable and outdoor exposure to  $WBGT_{max} > 30^{\circ}C$  has been associated with increased mortality rates among vulnerable populations (37). Accordingly, our exposure thresholds are a conservative estimator, yet comparable globally across spatial scales, of urban population exposure to extreme heat to capture the harmful social (73), health (1), economic (11, 12), and potential political consequences (74) of exposure to extreme heat.

### **Urban Population Exposure Trends**

We quantify urban exposure to extreme heat in person-days yr<sup>-1</sup> for each GHS-UCDB urban settlement from 1983 - 2016. Person-days yr<sup>-1</sup> is a widely used metric to compare and contrast exposure to extreme heat across geographies and time periods (4, 40, 75). For a given year ( $Y_i$ ) and for a given urban settlement ( $j$ ), we multiply the urban settlement's population ( $N_{ij}$ ) by the number of days for year  $i$  a threshold is exceeded (e.g.  $WBGT_{\max} > 30^{\circ}\text{C}$ ,  $Days_{ij}$ , eq. 13).

After summing exposure in person-days yr<sup>-1</sup> for each year at municipality, national, regional, and global scales, we evaluate annual rate of increase in exposure from 1983 – 2016 (person-days yr<sup>-1</sup>) across spatial scales by fitting simple ordinary least squares linear regression models (OLS). For example, at the municipality-level, we estimate the rate of change ( $\beta_{exp}$ ) from 1983 - 2016 in person-days yr<sup>-1</sup> as exposure ( $Exp_{ij}$ ) for year  $i$  from 1983 - 2016 with eq. 14.

$$Exp_{ij} = N_{ij} \times Days_{ij} \text{ (eq. 13)}$$

$$Exp_{ij} = \beta_0 + \beta_{exp} Y_i + \varepsilon \text{ (eq. 14)}$$

Next, we fit simple OLS regression models to estimate the rate of change in the number of days per year where a threshold is exceeded for each urban settlement (eq. 15). For both the rates of increase in exposure and days per year a threshold is exceeded we subset the data to include only urban settlements with statistically significant positive trends ( $p < 0.05$ ).

$$Warming_{ij} = \beta_0 + \beta_{j-days} Y_i + \varepsilon \text{ (eq. 15)}$$

### **Contribution to Exposure from Population Growth versus Total Urban Warming**

We quantify the share of exposure from population growth versus total urban warming for each urban settlement. For a given year  $i$  and urban settlement  $j$ , the share of person-days yr<sup>-1</sup>

from total urban warming ( $Heat_{ij}$ ) is calculated by multiplying the urban settlement's population fixed at 1983 by the number of days per year a threshold is exceeded (eq. 16).

$$Heat_{ij} = N_{83j} \times Days_{ij} \text{ (eq. 16)}$$

The share of exposure from population is calculated by multiplying  $Days_{ij}$  by the increase in population since 1983 (eq. 17).

$$Pop_{ij} = (N_{ij} - N_{83j}) \times Days_{ij} \text{ (eq. 17)}$$

To measure the rate of change in  $Heat_{ij}$  and  $Pop_{ij}$ , we apply simple OLS regressions to estimate the average rate of increase in person-days yr<sup>-1</sup>. The resulting coefficients,  $\beta_{pop}$  and  $\beta_{heat}$ , are the average rate of change in person-days yr<sup>-1</sup> from total urban warming and population growth, respectively. We use these coefficients to generate a bounded index to measure the relative share in the increase of exposure from urban population growth versus total urban warming from 1983 - 2016. To this end, for a given urban settlement  $j$ , we subtract the rate of person-day increase from population-growth ( $\beta_{pop}$ ) from the rate of person-day increase due to warming ( $\beta_{heat}$ ) and divide the result by the annual increase in coefficient of exposure ( $\beta_{exp}$ , eq. 18). We then normalize the index and plot the distribution of this index for at for all municipalities (Fig. 2C, Fig. S5C) and by region (Fig. 3, Fig. S6).

$$Index = (\beta_{pop} - \beta_{heat}) \div \beta_{exp} \text{ (eq. 18)}$$

### Identifying Heat Waves

Our dataset includes more than 150 million area-averaged daily  $T_{max}$ ,  $RH_{min}$ ,  $WBGT_{max}$ , and  $HI_{max}$  observations spanning more than 13,000 urban settlements from 1983 to 2016. As

such, we produced a comprehensive inventory of urban extreme heat events across the two thresholds employed, for all urban settlements as a derivative product that identifies the duration, intensity, magnitude and dates of all urban extreme heat events worldwide from 1983 - 2016. The entire dataset is searchable by English-language municipality names, country, and region (including sub- and intermediate-regions) and made publicly available for scholars and practitioners to identify extreme heat events based on the criteria of their choosing (22).

### **Uncertainty and Limitations**

We recognize that, aside from our linear regression models, the results are presented as point estimates without uncertainty. Yet all of the underlying data are from complex fusions of various different data sources. The underlying data products being used lack characterization of uncertainty and thus prevent us from estimating uncertainty in our results. Because of this, our analysis focuses on distinct and extreme differences in the patterns we identify that are representative estimates of the true signals of the underlying processes. Given the fine-grained spatiotemporal resolution of our analysis, our results provide crucial improvements of previous coarse-scale data on total urban warming (4, 40) and urban population growth trends (27) that are key for future climate change scenario planning (21), adaptation development (6) and early warning system development (20).

### **Data and materials availability**

All data and code produced are publicly available on Github: <https://github.com/ecohydro/GlobalUrbanHeat>. CHIRTS-daily  $T_{\max}$  and the relative humidity product are available from UCSB Climate Hazard Center FTP site: [ftp://ftp.chc.ucsb.edu/pub/org/chc/products/CHIRTSdaily/v1.0/global\\_tifs\\_p05/](ftp://ftp.chc.ucsb.edu/pub/org/chc/products/CHIRTSdaily/v1.0/global_tifs_p05/)



Global Human Settlement Layer Urban Centers Database (GHS-UCDB) is available from the European Commission JRC: <https://ghsl.jrc.ec.europa.eu/datasets.php>

**Acknowledgments:** The authors would like to thank Prof. Susan Cassels for providing an internal review of this manuscript and the Earth Research Institute computing staff for the tireless assistance throughout this project. We also thank two anonymous reviewers for their excellent feedback. CT was supported by the UC Presidential Dissertation Year Fellowship through UC Santa Barbara and the Earth Institute Postdoctoral Fellowship Program, Columbia University. CT, KC and TE, received support from NSF awards SES-1801251, SES-1832393, DEB-1924309. Support for CF and PP came from the National Aeronautics and Space Administration (NASA) GPM mission grant #80NSSC19K0686, the United States Agency for International Development (USAID) cooperative agreement #72DFFP19CA00001 and the Famine Early Warning Systems Network and the Defense Advanced Research Projects Agency (DARPA) World Modelers Program under Army Research Office (ARO) prime contract no. W911NF-18-1-0018.

## References and Notes:

1. N. Watts, *et al.*, The 2020 report of The Lancet Countdown on health and climate change: responding to converging crises. *Lancet* **397**, 129–170 (2021).
2. E. Coffel, R. M. Horton, A. M. De Sherbinin, Temperature and humidity based projections of a rapid rise in global heat stress exposure during the 21st century (2017).
3. C. Mora, *et al.*, Global risk of deadly heat. *Nat. Clim. Chang.* **7**, 501 (2017).
4. T. K. R. Matthews, R. L. Wilby, C. Murphy, Communicating the deadly consequences of global warming for human heat stress. *Proc. Natl. Acad. Sci. U. S. A.* **114**, 3861–3866 (2017).
5. G. A. Meehl, C. Tebaldi, More intense, more frequent, and longer lasting heat waves in the 21st century. *Science* **305**, 994–997 (2004).
6. G. Manoli, *et al.*, Magnitude of urban heat islands largely explained by climate and population. *Nature* **573**, 55–60 (2019).
7. E. D. Coffel, A. de Sherbinin, R. M. Horton, K. Lane, The Science of Adaptation to Extreme Heat. *Resilience* (2018).
8. H. Wouters, *et al.*, Heat stress increase under climate change twice as large in cities as in rural areas: A study for a densely populated midlatitude maritime region. *Geophys. Res. Lett.* **44**, 8997–9007 (2017).
9. T. R. Oke, Canyon geometry and the nocturnal urban heat island: Comparison of scale model and field observations. *J. Climatol.* **1**, 237–254 (1981).
10. E. Day, S. Fankhauser, N. Kingsmill, H. Costa, A. Mavrogianni, Upholding labour productivity under climate change: an assessment of adaptation options. *Clim. Policy* **19**, 367–385 (2019).
11. M. Burke, S. M. Hsiang, E. Miguel, Global non-linear effect of temperature on economic production. *Nature* **527**, 235–239 (2015).

12. T. A. Carleton, *et al.*, Valuing the Global Mortality Consequences of Climate Change Accounting for Adaptation Costs and Benefits (2020) <https://doi.org/10.3386/w27599>.
13. T. Chakraborty, A. Hsu, D. Manya, G. Sheriff, Disproportionately higher exposure to urban heat in lower-income neighborhoods: a multi-city perspective. *Environ. Res. Lett.* **14**, 105003 (2019).
14. E. B. Wetherley, J. P. McFadden, D. A. Roberts, Megacity-scale analysis of urban vegetation temperatures. *Remote Sens. Environ.* **213**, 18–33 (2018).
15. F. Estrada, W. J. W. Botzen, R. S. J. Tol, A global economic assessment of city policies to reduce climate change impacts. *Nat. Clim. Chang.* **7**, 403 (2017).
16. C. Tuholske, K. Caylor, T. Evans, R. Avery, Variability in urban population distributions across Africa. *Environ. Res. Lett.* **14**, 085009 (2019).
17. C. Raymond, T. Matthews, R. M. Horton, The emergence of heat and humidity too severe for human tolerance. *Science Advances* **6**, eaaw1838 (2020).
18. A. M. Broadbent, E. S. Krayenhoff, M. Georgescu, The motley drivers of heat and cold exposure in 21st century US cities. *Proc. Natl. Acad. Sci. U. S. A.* **117**, 21108–21117 (2020).
19. J. K. Vanos, J. W. Baldwin, O. Jay, K. L. Ebi, Simplicity lacks robustness when projecting heat-health outcomes in a changing climate. *Nat. Commun.* **11**, 6079 (2020).
20. E. C. De Perez, *et al.*, Global predictability of temperature extremes. *Environ. Res. Lett.* **13**, 054017 (2018).
21. B. C. O’Neill, *et al.*, Achievements and needs for the climate change scenario framework. *Nat. Clim. Chang.* **10**, 1074–1084 (2020).
22. T. T. Smith, B. F. Zaitchik, J. M. Gohlke, Heat waves in the United States: definitions, patterns and trends. *Clim. Change* **118**, 811–825 (2013).
23. A. Verdin, *et al.*, Development and validation of the CHIRTS-daily quasi-global high-resolution daily temperature data set. *Sci Data* **7**, 303 (2020).
24. C. Funk, P. Peterson, S. Peterson, S. Shukla, A High-Resolution 1983–2016 Tmax Climate Data Record Based on Infrared Temperatures and Stations by the Climate Hazard Center. *Journal of Climate* **32**, 5639–5658 (2019).
25. N. Watts, *et al.*, The 2019 report of The Lancet Countdown on health and climate change: ensuring that the health of a child born today is not defined by a changing climate. *Lancet* **394**, 1836–1878 (2019).
26. Copernicus Climate Change Service (C3S), ERA5: Fifth generation of ECMWF atmospheric reanalysis of the global climate (2017).
27. UN-DESA, World Urbanization Prospects 2018 (2018) (August 30, 2018).
28. S. Russo, J. Sillmann, A. Sterl, Humid heat waves at different warming levels. *Sci. Rep.* **7**, 7477 (2017).
29. A. J. Florczyk, M. Melchiorri, C. Corbane, M. Schiavina, Description of the GHS Urban Centre Database 2015 (2019).

30. ISO, ISO 7243: Ergonomics of the thermal environment—assessment of heat stress using the wbg (wet bulb globe temperature) index. *Int Org Standard Geneva Switzerland* (2017).
31. NOAA, The Heat Index Equation (28-May-2014) (04-April-2020).
32. K. R. Spangler, K. R. Weinberger, G. A. Wellenius, Suitability of gridded climate datasets for use in environmental epidemiology. *J. Expo. Sci. Environ. Epidemiol.* **29**, 777–789 (2019).
33. A. A. Scott, D. W. Waugh, B. F. Zaitchik, Reduced Urban Heat Island intensity under warmer conditions. *Environ. Res. Lett.* **13** (2018).
34. M. Georgescu, P. E. Morefield, B. G. Bierwagen, C. P. Weaver, Urban adaptation can roll back warming of emerging megapolitan regions. *Proc. Natl. Acad. Sci. U. S. A.* **111**, 2909–2914 (2014).
35. S. S. Cheung, J. K. W. Lee, J. Oksa, Thermal stress, human performance, and physical employment standards. *Appl. Physiol. Nutr. Metab.* **41**, S148–64 (2016).
36. K. Parsons, Heat stress standard ISO 7243 and its global application. *Ind. Health* **44**, 368–379 (2006).
37. B. Pradhan, *et al.*, Heat Stress Impacts on Cardiac Mortality in Nepali Migrant Workers in Qatar. *Cardiology* **143**, 37–48 (2019).
38. A. Verdin, K. Grace, F. Davenport, C. Funk, G. Husak, Can we advance individual-level heat-health research through the application of stochastic weather generators? *Clim. Change* **164** (2021).
39. NWS Internet Services Team, Excessive Heat Warning (March 8, 2021).
40. G. Rohat, J. Flacke, A. Dosio, H. Dao, M. Maarseveen, Projections of Human Exposure to Dangerous Heat in African Cities Under Multiple Socioeconomic and Climate Scenarios. *Earth's Future* **121**, 1111 (2019).
41. , “Economic 1998-2017 Losses, Poverty & Disasters” (UNISDR/CRED).
42. R. Hoffmann, A. Dimitrova, R. Muttarak, J. Crespo Cuaresma, J. Peisker, A meta-analysis of country-level studies on environmental change and migration. *Nat. Clim. Chang.* (2020) <https://doi.org/10.1038/s41558-020-0898-6>.
43. A. Zimmer, *et al.*, Dynamics of population growth in secondary cities across southern Africa. *Lands. Ecol.* **35**, 2501–2516 (2020).
44. J. V. Henderson, A. Storeygard, U. Deichmann, Has climate change driven urbanization in Africa? *J. Dev. Econ.* **124**, 60–82 (2017).
45. R. Black, S. R. G. Bennett, S. M. Thomas, J. R. Beddington, Climate change: Migration as adaptation. *Nature* **478**, 447–449 (2011).
46. S. Kumar, India’s heat wave and rains result in massive death toll. *Lancet* **351**, 1869 (1998).
47. T. E. Bernard, I. Iheanacho, Heat index and adjusted temperature as surrogates for wet bulb globe temperature to screen for occupational heat stress. *J. Occup. Environ. Hyg.* **12**, 323–333 (2015).
48. C. P. Kelley, S. Mohtadi, M. A. Cane, R. Seager, Y. Kushnir, Climate change in the Fertile Crescent and implications of the recent Syrian drought. *Proc. Natl. Acad. Sci. U. S. A.* **112**, 3241–3246 (2015).

49. F. G. Kuglitsch, *et al.*, Heat wave changes in the eastern Mediterranean since 1960: HEAT WAVES IN THE EASTERN MEDITERRANEAN. *Geophys. Res. Lett.* **37**, 529 (2010).
50. D. Helman, B. F. Zaitchik, C. Funk, Climate has contrasting direct and indirect effects on armed conflicts. *Environ. Res. Lett.* (2020).
51. H. Buhaug, Climate-conflict research: some reflections on the way forward. *Wiley Interdisciplinary Reviews: Climate Change* **6**, 269–275 (2015).
52. R. G. Steadman, The Assessment of Sultriness. Part II: Effects of Wind, Extra Radiation and Barometric Pressure on Apparent Temperature. *J. Appl. Meteorol. Climatol.* **18**, 874–885 (1979).
53. A. Casanueva, *et al.*, Overview of Existing Heat-Health Warning Systems in Europe. *Int. J. Environ. Res. Public Health* **16** (2019).
54. , 1990-6-26 Phoenix, AZ Weather History. <https://www.wunderground.com/history/daily/KPHX/date/1990-6-26>. *Weather Underground*. (June 10, 2021).
55. A. Minkler, At 118 degrees, Thursday heat in Phoenix breaks daily record set in 1934. *The Arizona Republic* (2020) (June 18, 2021).
56. L. E. Watkins, *et al.*, Extreme heat vulnerability in Phoenix, Arizona: A comparison of all-hazard and hazard-specific indices with household experiences. *Appl. Geogr.* **131**, 102430 (2021).
57. W.-C. Chuang, P. Gober, Predicting hospitalization for heat-related illness at the census-tract level: accuracy of a generic heat vulnerability index in Phoenix, Arizona (USA). *Environ. Health Perspect.* **123**, 606–612 (2015).
58. T. Kjellstrom, Impact of Climate Conditions on Occupational Health and Related Economic Losses: A New Feature of Global and Urban Health in the Context of Climate Change. *Asia. Pac. J. Public Health* **28**, 28S–37S (2016).
59. P. Zhang, O. Deschenes, K. Meng, J. Zhang, Temperature effects on productivity and factor reallocation: Evidence from a half million chinese manufacturing plants. *J. Environ. Econ. Manage.* **88**, 1–17 (2018).
60. World Bank, Population living in slums (% of urban population) | Data (2019) (October 26, 2019).
61. S. Fox, Urbanization as a Global Historical Process: Theory and Evidence from sub-Saharan Africa. *Popul. Dev. Rev.* **38**, 285–310 (2012).
62. , List of Stations. *Berkeley Earth* (September 11, 2020).
63. J. Sheffield, G. Goteti, E. F. Wood, Development of a 50-Year High-Resolution Global Dataset of Meteorological Forcings for Land Surface Modeling. *J. Clim.* **19**, 3088–3111 (2006).
64. D. Bolton, The Computation of Equivalent Potential Temperature. *Mon. Weather Rev.* **108**, 1046–1053 (1980).
65. A. Cattaneo, A. Nelson, Global mapping of urban–rural catchment areas reveals unequal access to services. *Proceedings of the* (2021).
66. D. L. Balk, M. R. Montgomery, Guest Editorial: “Spatializing Demography for the Urban Future.” *Spatial Demography* **3**, 59–62 (2015).

67. K. Parsons, *Human Thermal Environments: The Effects of Hot, Moderate, and Cold Environments on Human Health, Comfort, and Performance, Third Edition* (CRC Press, 2014).
68. G. D. Bynum, *et al.*, Induced hyperthermia in sedated humans and the concept of critical thermal maximum. *Am. J. Physiol.* **235**, R228–36 (1978).
69. S. S. Cheung, T. M. McLellan, Heat acclimation, aerobic fitness, and hydration effects on tolerance during uncompensable heat stress. *J. Appl. Physiol.* **84**, 1731–1739 (1998).
70. A. Bouchama, *et al.*, Inflammatory, hemostatic, and clinical changes in a baboon experimental model for heatstroke. *J. Appl. Physiol.* **98**, 697–705 (2005).
71. K. B. Pandolf, R. F. Goldman, Convergence of skin and rectal temperatures as a criterion for heat tolerance. *Aviat. Space Environ. Med.* **49**, 1095–1101 (1978).
72. S. C. Sherwood, M. Huber, An adaptability limit to climate change due to heat stress. *Proc. Natl. Acad. Sci. U. S. A.* **107**, 9552–9555 (2010).
73. M. Burke, *et al.*, Higher temperatures increase suicide rates in the United States and Mexico. *Nat. Clim. Chang.* **8**, 723–729 (2018).
74. S. M. Hsiang, K. C. Meng, M. A. Cane, Civil conflicts are associated with the global climate. *Nature* **476**, 438–441 (2011).
75. G. Ceccherini, S. Russo, I. Amezttoy, Heat waves in Africa 1981–2015, observations and reanalysis. *Nat. Hazards* (2017).

## Figure Legends

**Fig. 1.** Global urban population exposure to extreme heat, defined by one day or long periods where WBGT<sub>max</sub> >30°C, from 1983 – 2016 (A), with the contribution from population growth (B) and total urban warming (C) decoupled.

**Fig. 2.** (A) Municipality-level increase in the rate of urban population exposure to extreme heat from 1983 - 2016 and (B) the rate of increase in the total number of days per year where WBGT<sub>max</sub> > 32°C. (C) The share of population versus total urban warming in the rate of increase of total population exposure using WBGT<sub>max</sub> > 30°C. Fig. S4 zooms in on Southern India, Ganges Delta, Nile river valley and delta, and Tigres-Euphrates river valley. Note, the largest

increase in exposure (A) and days per year WBGT >30°C (B) are rendered last for emphasis. In (C), urban settlements with a greater contribution from total urban warming (e.g. pink) are rendered last for emphasis.

**Fig. 3.** The comparative contribution to the increase in the rate of urban exposure to extreme heat due to population growth versus total urban warming varies considerably across selected regions using WBGT<sub>max</sub> > 30 °C threshold.

**Fig. 4** Two examples – Kolkata, India in 1998 (A and B) and Aleppo, Syria in 2010 (C and D) – previously poorly or undocumented documented urban heat waves that our analysis uncovered. In both cases, the contrast between daily HI<sub>max</sub> (A and C) with WBGT<sub>max</sub> (B and D) estimates shows that, while HI was not designed to be accurate at values HI<sub>max</sub> > 50°C, WBGT<sub>max</sub> does not capture the amplitude of daily extremely hot temperature-humidity combinations.

**Figure 1**

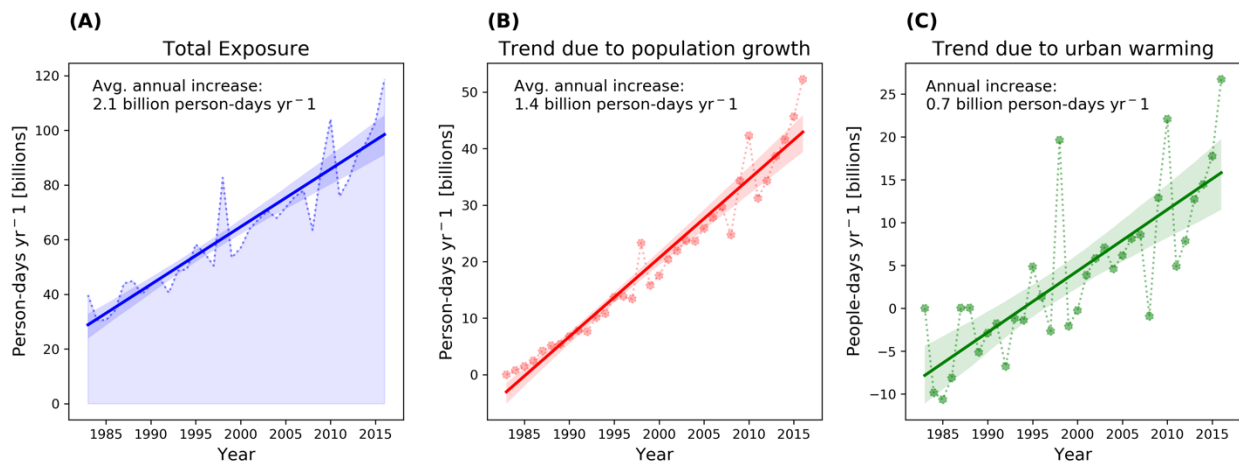


**Figure 2**

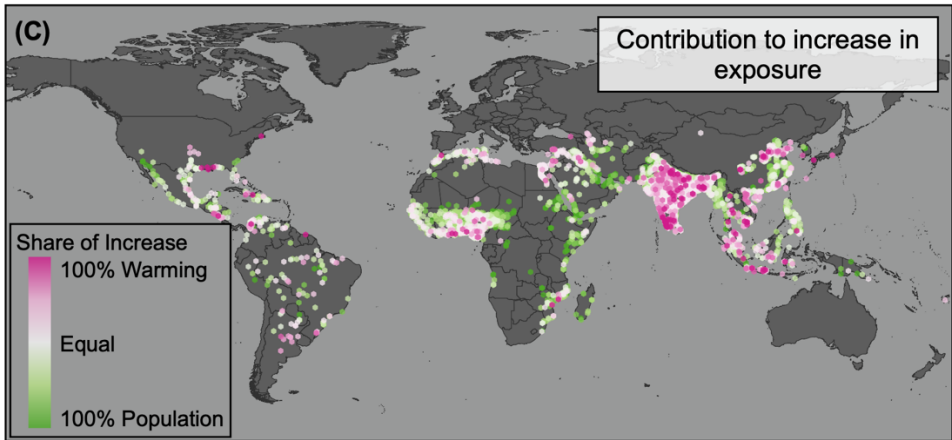
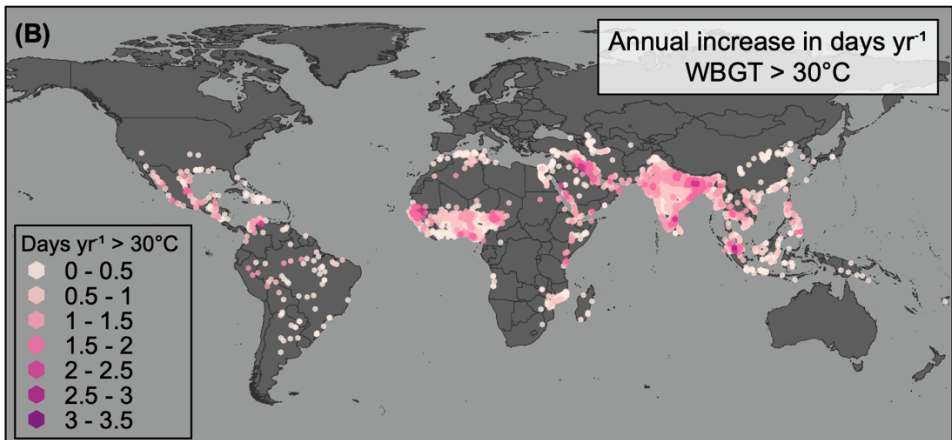
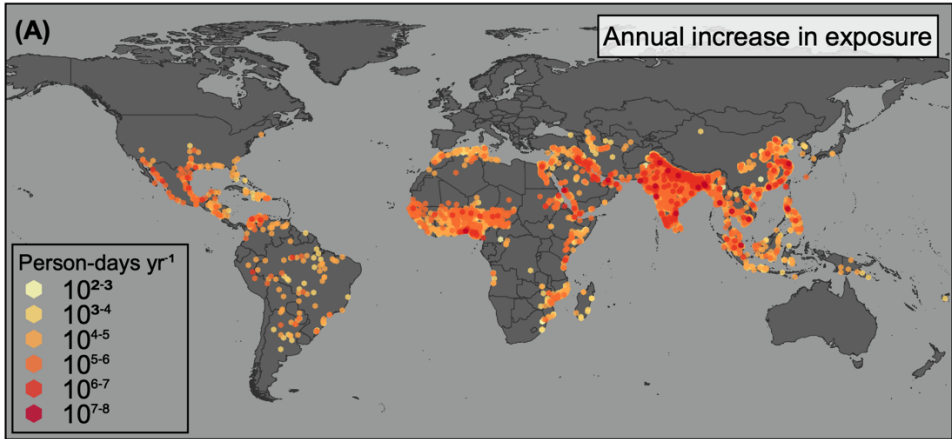




**Figure 3**

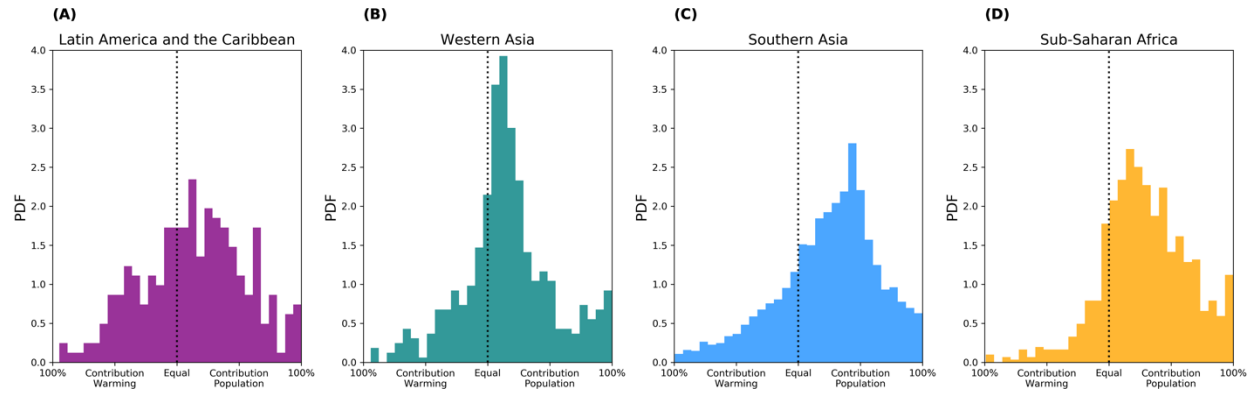
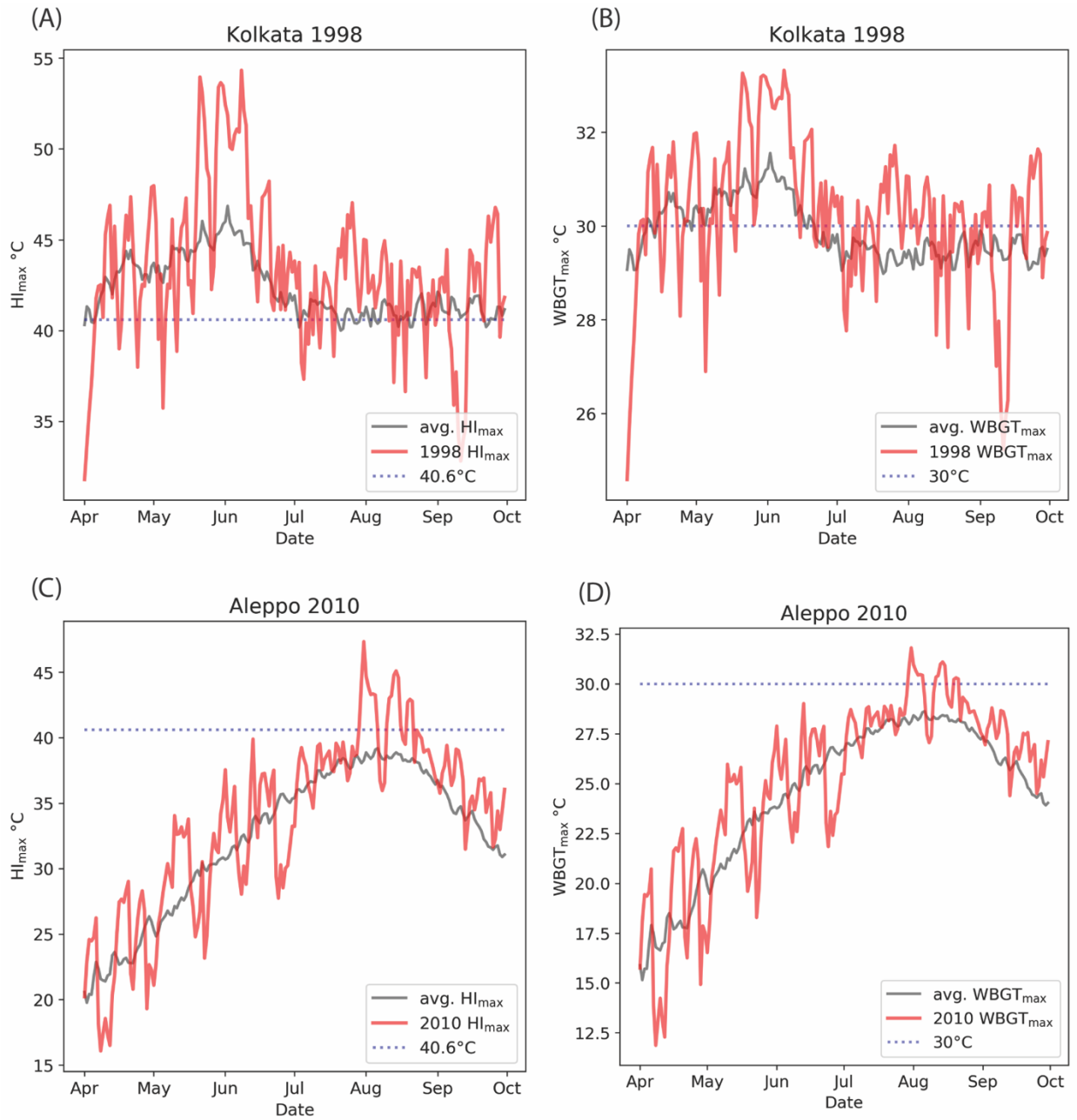


**Figure 4**



# Supplementary Information for

Global Urban Population Exposure to Extreme Heat

Cascade Tuholske, Kelly Caylor, Chris Funk, Andrew Verdin, Stuart Sweeney, Kathryn Grace, Pete Peterson, and Tom Evans

Correspondence to: [cascade@ucsb.edu](mailto:cascade@ucsb.edu)

**This PDF file includes:**

Supplementary text  
Figures S1 to S11  
Tables S1 to S4  
SI References

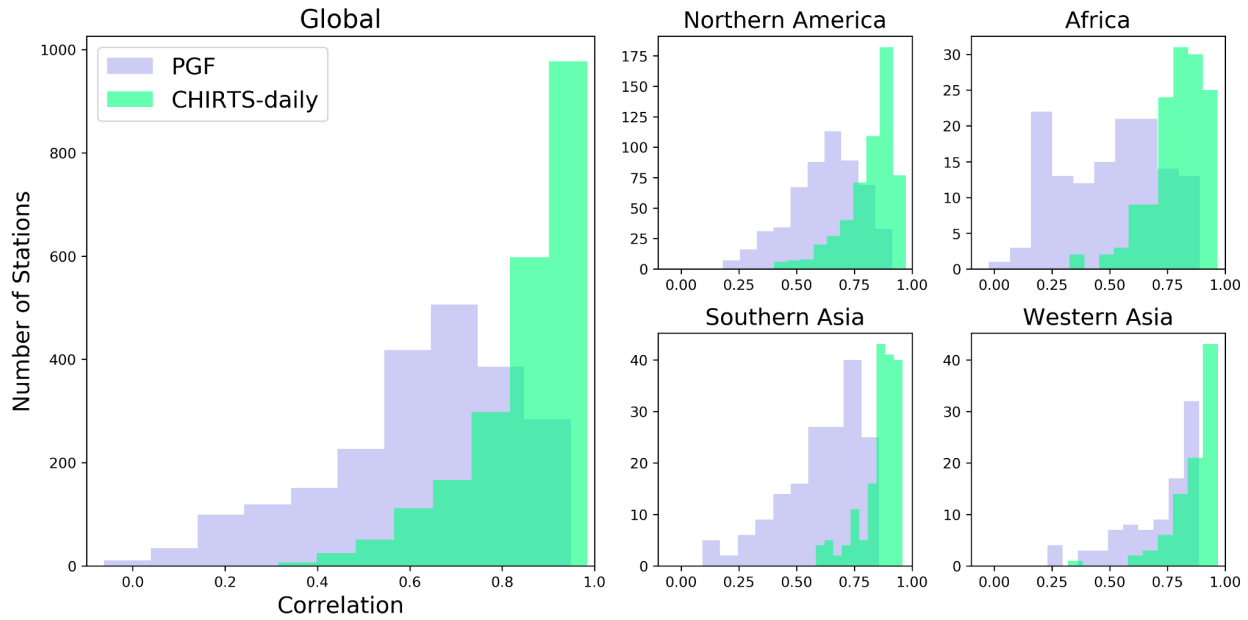
### Supplementary Text

Fig. S7 provides examples of exposure trends at the country-level for Nigeria, China and Italy, separating the contribution from total urban warming and urban population growth as shown globally in Figure 1 of the main text. These three examples highlight how geographic variation—including levels of development, country population sizes, and urban settlements located across a range of climate zones within each country (1)—affect national-level exposure trajectories. Both China and Nigeria are both rapidly urbanizing (2). As such, urban population growth explains much of the national-level exposure trajectories. Unlike in China, where the national-level contribution from total urban warming is less pronounced (Fig. S7), we find that in Nigeria the exposure trajectory is also clearly being affected by total urban warming (Fig. S7). In Italy, populations across all urban settlements are stable or declining (2). Thus, any increase in total urban warming will drive the overall increase in exposure (Fig. S7).

As we zoom into municipality-level exposure, our analysis reveals heterogeneous spatial patterns of how urban population growth and total urban warming drive exposure trajectories within a given country, especially those that span climate gradients (Fig. S8). Take three examples of large Nigerian cities (Fig S8): Lagos, Abuja, and Kano. These three cities cover diverse climate zones across Nigeria's north-south gradient. While all three have experienced rapid population growth since 1983, the trend for exposure and total urban warming varies across the three cities. For Lagos, which is coastal, the effect of the annual increase in the number of days per year where  $WBGT_{max} > 30^{\circ}C$  on the city's exposure trajectory is apparent. Similarly, Kano, which is in the north and borders the Sahara Desert, has experienced a more rapid increase in the number of days per year where  $WBGT_{max} > 30^{\circ}C$ . In contrast, Abuja, which is centrally located and experienced rapid population growth like Lagos and Kano, rarely experienced any days from 1983 - 2016 where  $WBGT_{max} > 30^{\circ}C$  and thus it has no significant exposure trend.

The contrast in exposure trajectories between countries and across urban settlements within a country highlights the importance of fine-resolution, yet globally comprehensive urban extreme heat exposure analysis presented here. Indeed, our results and data capture the diverse spatial patterns requisite to pinpoint and compare exposure trajectories to aid the development of adaptation strategies (1) and early warning systems (3). This is especially important given finite resources and the various tradeoffs of adaptation to reduce the impacts of urban extreme heat exposure (4, 5).

**Fig. S1** Distribution of correlation statistics ( $R^2$ ) for urban CHIRTS-daily  $T_{\max}$  and



Princeton University's Global Meteorological Forcing Dataset (PGF)  $T_{\max}$  with urban Global Historical Climatology Network and Global Summary of the Day databases. CHIRTS-daily  $T_{\max}$  outperforms PGF globally and in crucial rapidly urbanizing regions, such as Africa, Southern Asia, Western Asia, that lack station observations for the majority of urban settlements (Fig. S3). Figure was reconstructed with data from (4).

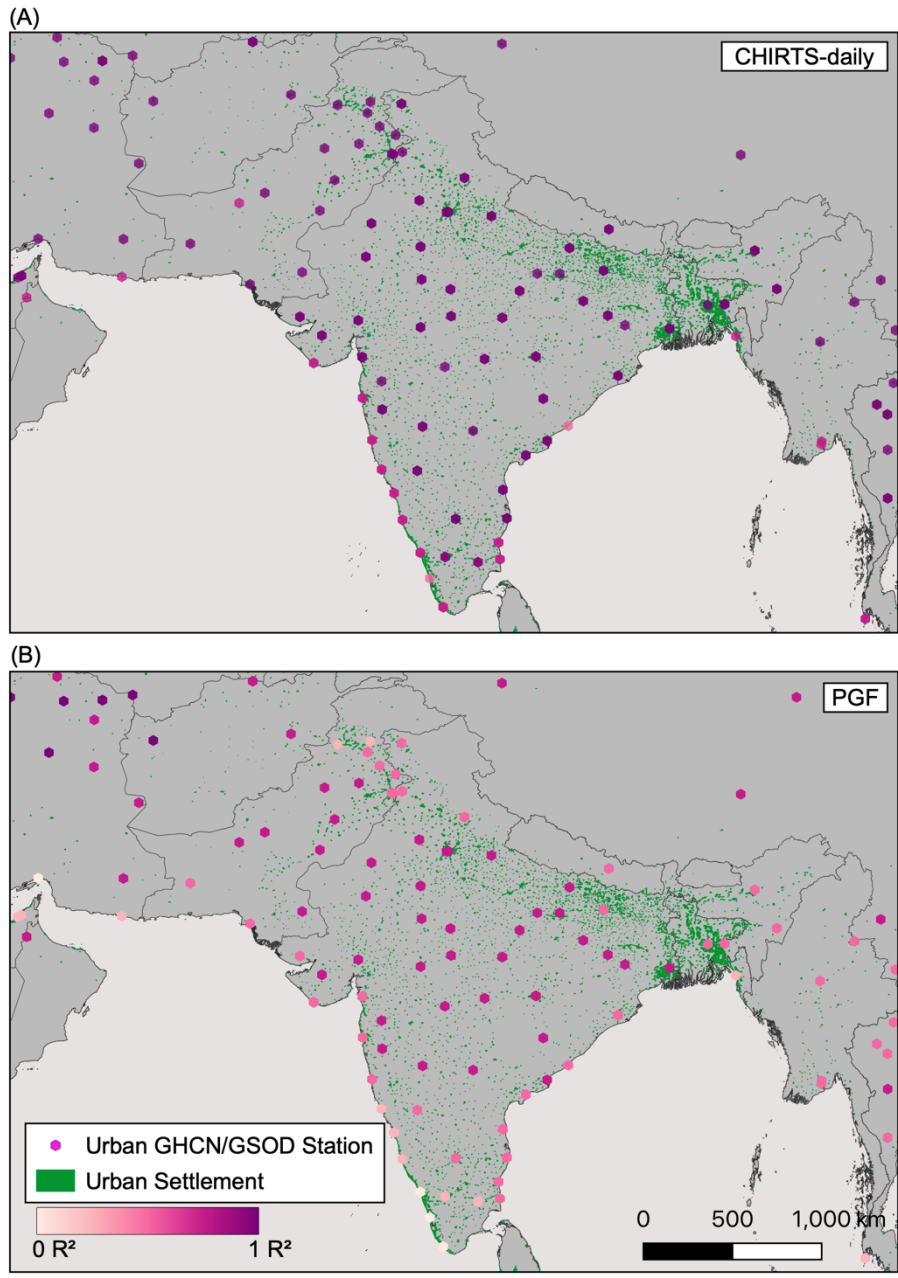


**Fig. S2.** Correlation ( $R^2$ ) for CHIRTS-daily  $T_{max}$  and Princeton University’s Global Meteorological Forcing Dataset (PGF)  $T_{max}$  with urban Global Historical Climatology Network and Global Summary of the Day databases for Southern Asia. Much of the region’s urban areas lack station observations. For example, in India, of 3,248 urban

settlements, only 111 have GHCN/GSOD stations with a robust reporting record (4). At 0.05° spatial resolution, CHIRTS-daily provides accurate, high resolution urban  $T_{max}$  estimates for rapidly urbanizing regions like Southern Asia that lack widespread urban station observations and improves over previous datasets like PGF.

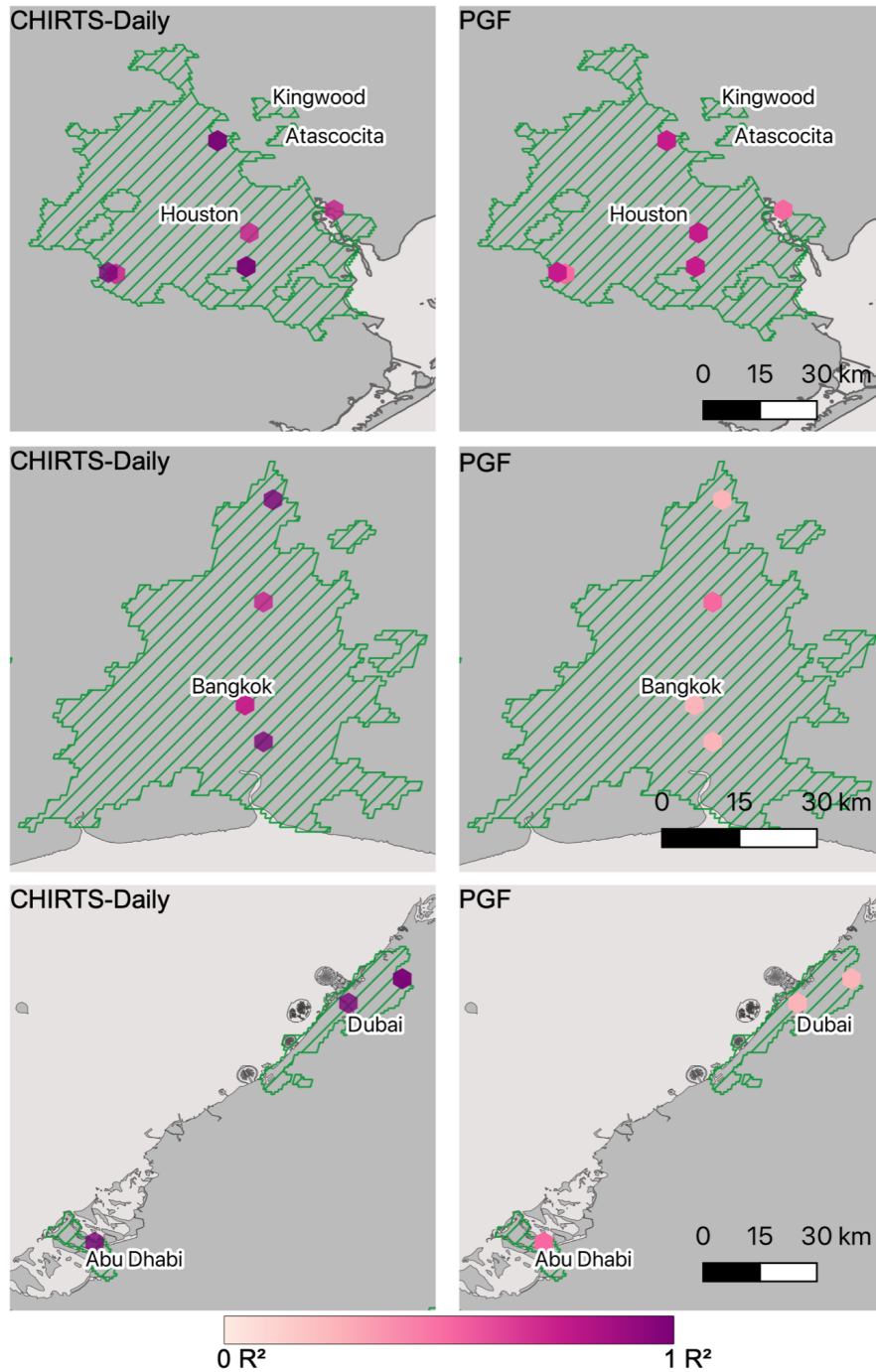


**Fig. S3** Correlation ( $R^2$ ) for CHIRTS-daily  $T_{max}$  and Princeton University's Global Meteorological Forcing Dataset (PGF)  $T_{max}$  with urban Global Historical Climatology

Network and Global Summary of the Day databases for the Houston, Bangkok, Dubai, and Abu Dhabi metropolitan areas. All four urban settlements had a significant exposure trend from 1983 - 2016 using a threshold of  $WBGT_{max} > 30^{\circ}C$ . Across these diverse urban contexts, CHIRTS-daily better captures the urban  $T_{max}$  signal than PGF and provides accurate  $T_{max}$  estimates.

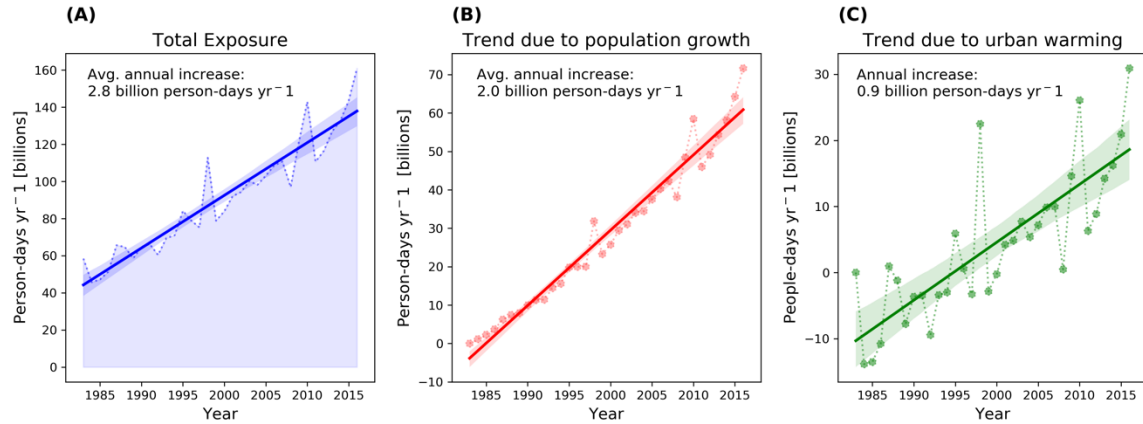


**Fig. S4.** Global urban population exposure to extreme heat from 1983 – 2016 (A), with the contribution from population growth (B) and total urban warming (C) decoupled. Extreme heat exposure is defined by urban population exposed to two days or longer periods where  $HI_{max} > 40.6^{\circ}C$ .



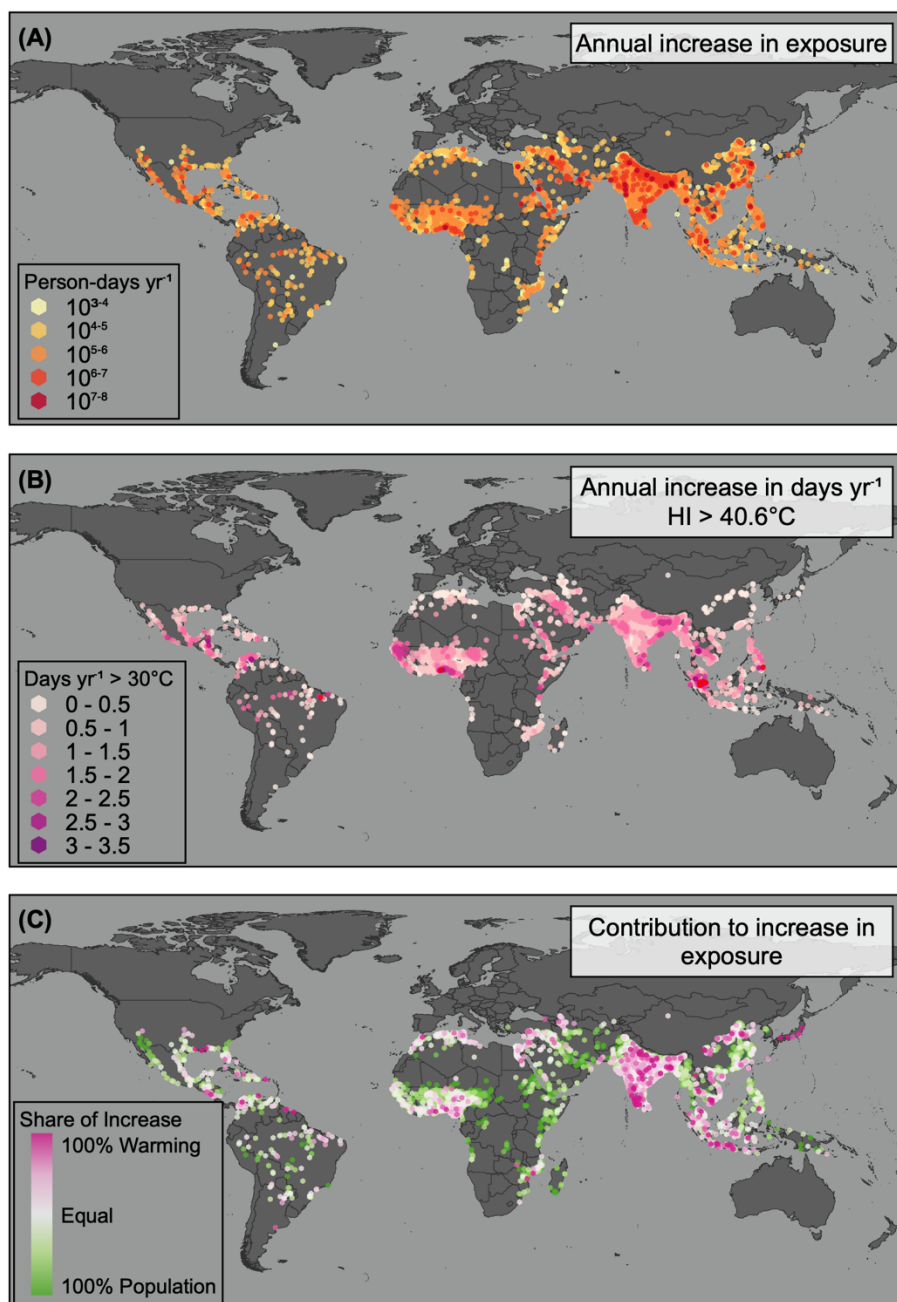


**Fig. S5.** (A) Municipality-level increase in the rate of urban population exposure to extreme heat from 1983 - 2016 and (B) the rate of increase in the total number of days per year where  $HI_{\max} > 40.6^{\circ}\text{C}$  (C). Note, the largest increase in exposure (A) and days per year  $HI_{\max} > 40.6^{\circ}\text{C}$  (B) are rendered last for emphasis. In (C), urban settlements with a greater contribution from total urban warming (e.g. pink) are rendered last for emphasis. Extreme heat exposure is defined by urban population exposed to two days or longer periods where  $HI_{\max} > 40.6^{\circ}\text{C}$ .

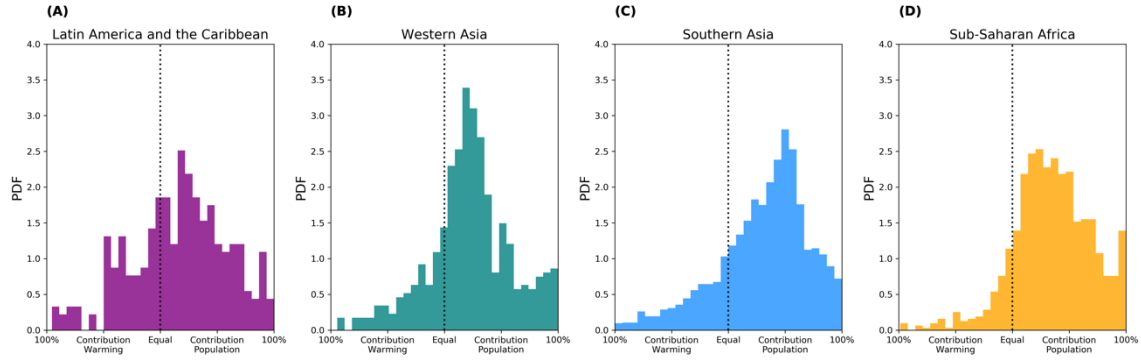


**Fig. S6.** The comparative contribution to the increase in the rate of urban exposure to extreme heat due to population growth versus total urban warming varies considerably across selected regions when extreme heat exposure is defined by urban population exposed to two days or longer periods where  $HI_{\max} > 40.6^{\circ}\text{C}$ .

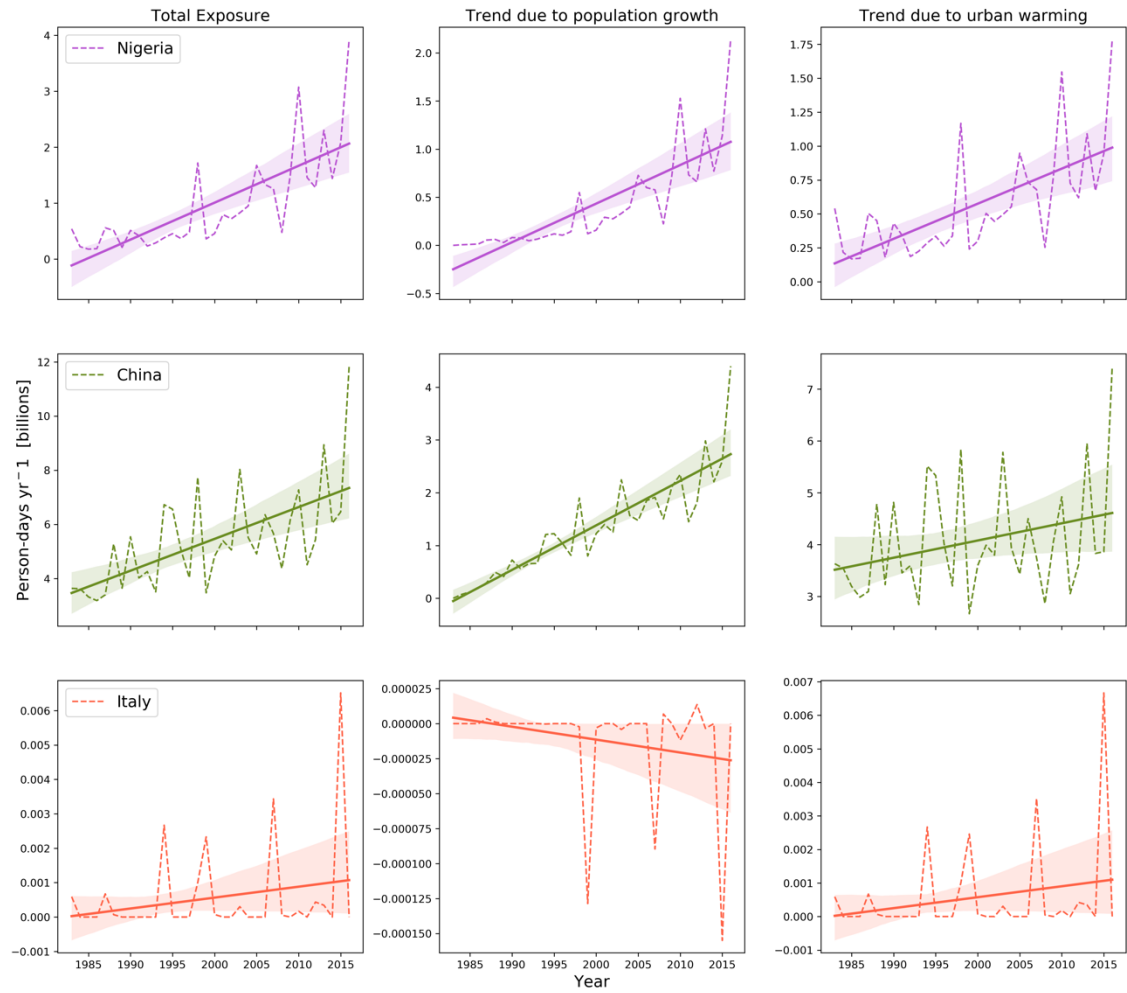


**Fig. S7.** National-level total urban warming exposure trajectories from 1983 – 2016 with the contribution from total urban warming and urban population growth separated for Nigeria, China and Italy.  $WBGT_{max} > 30^{\circ}C$  threshold is used to define extreme heat exposure.

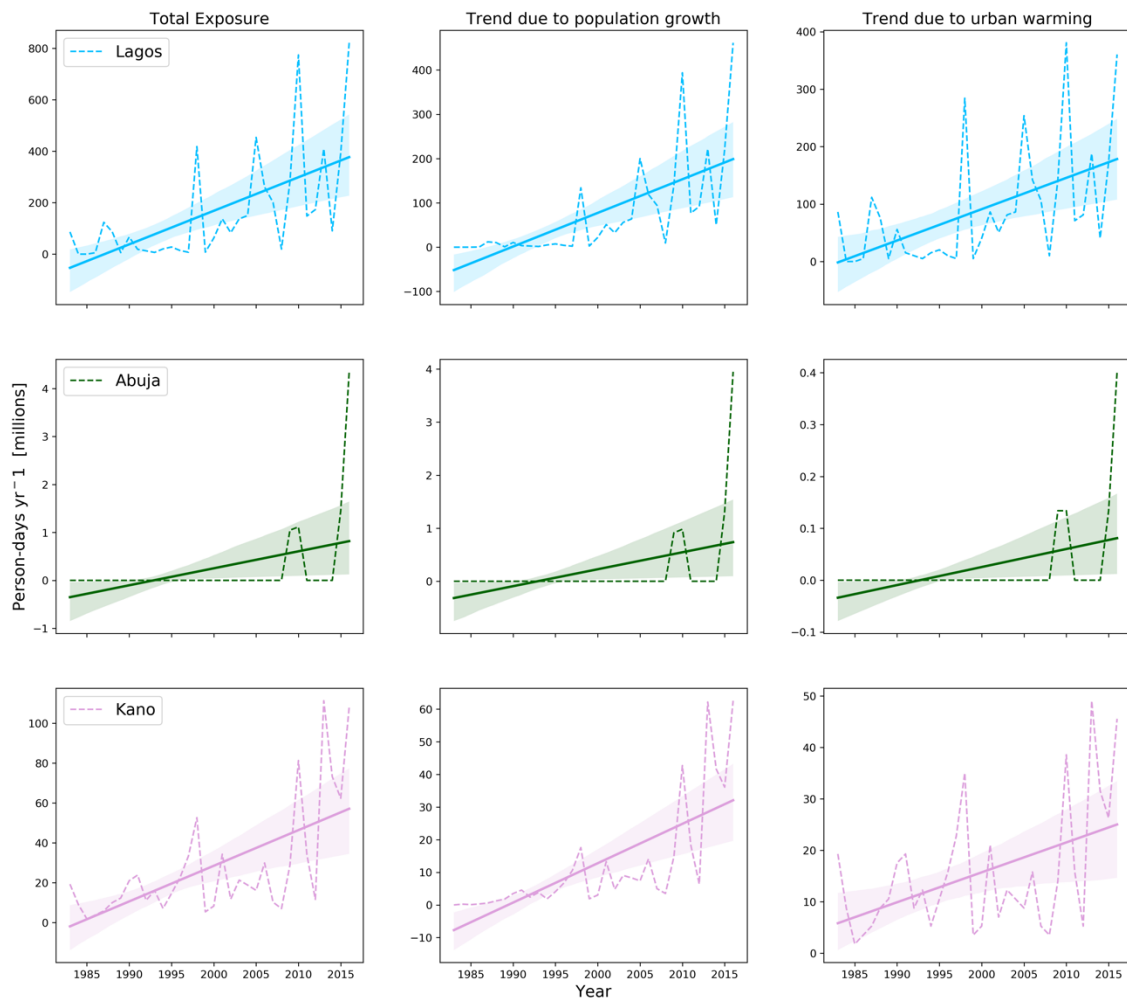


**Fig. S8.** Municipality-level total urban warming exposure trajectories from 1983 – 2016 with the contribution from total urban warming and urban population growth separated for three large Nigerian cities—Lagos, Abuja, and Kano.  $WBGT_{max} > 30^{\circ}C$  threshold is used to define extreme heat exposure.

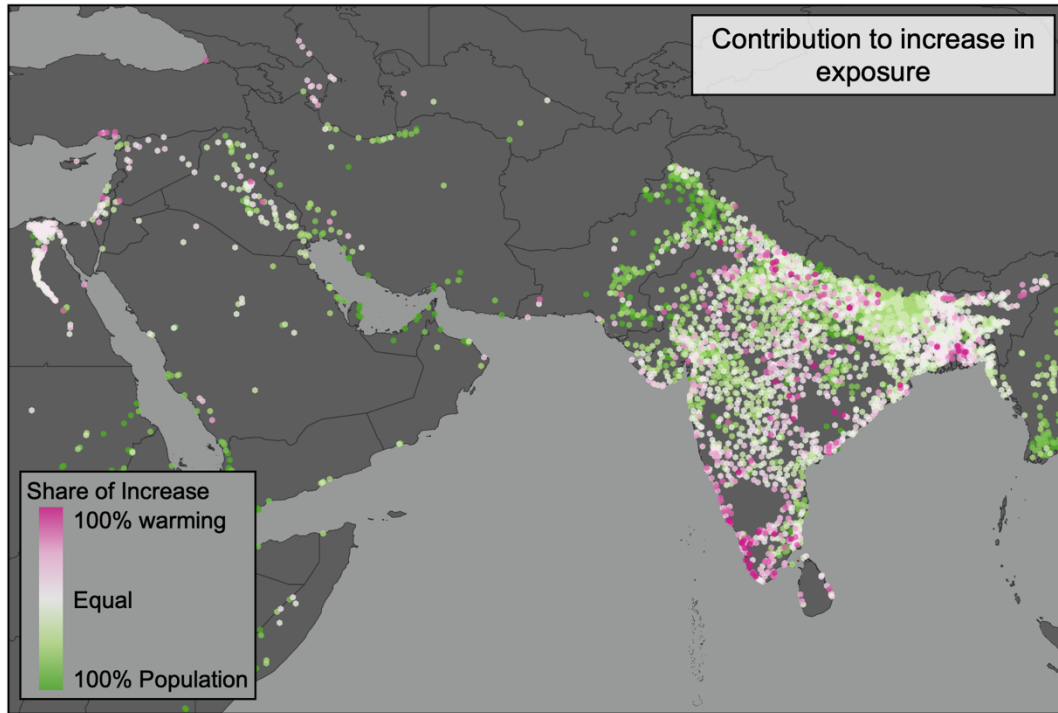


**Fig. S9.** Zoomed in from Fig. 2C. The share of population versus total urban warming in the rate of increase of total population exposure in Southern India, Ganges Delta, Nile river valley and delta, and Tigris-Euphrates river valley using  $WBGT_{max} > 30^{\circ}C$ . Total urban warming drove exposure trajectories in urban settlements in coastal southwestern India and southern Indonesia, though rapidly urbanizing regions. Note, urban settlements with a greater contribution from total urban warming (e.g. pink) are rendered last for emphasis.  $WBGT_{max} > 30^{\circ}C$  threshold is used to define extreme heat exposure.

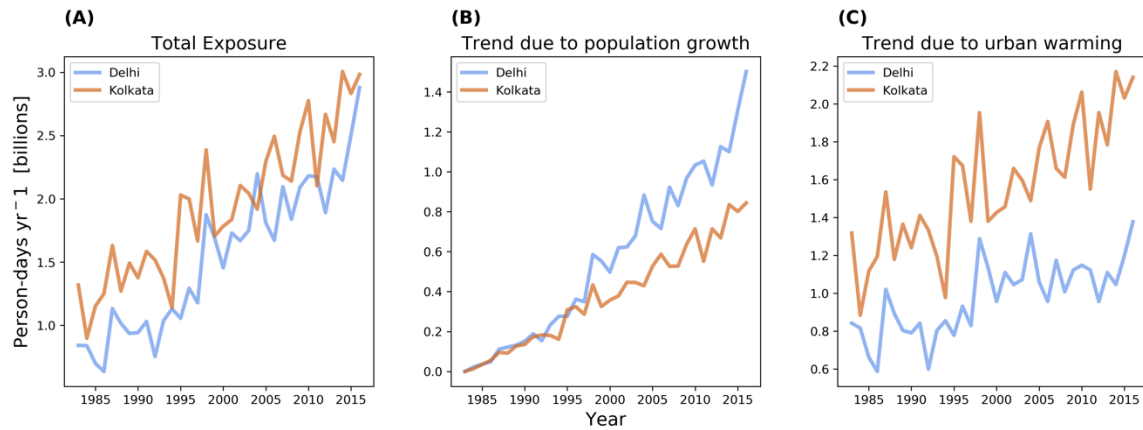


**Fig. S10.** (A) Total urban population exposure to extreme heat from 1983 – 2016 for Delhi and Kolkata, with the contribution from (B) population growth and (C) total urban warming decoupled.  $WBGT_{max} > 30^{\circ}C$  threshold is used to define extreme heat exposure.

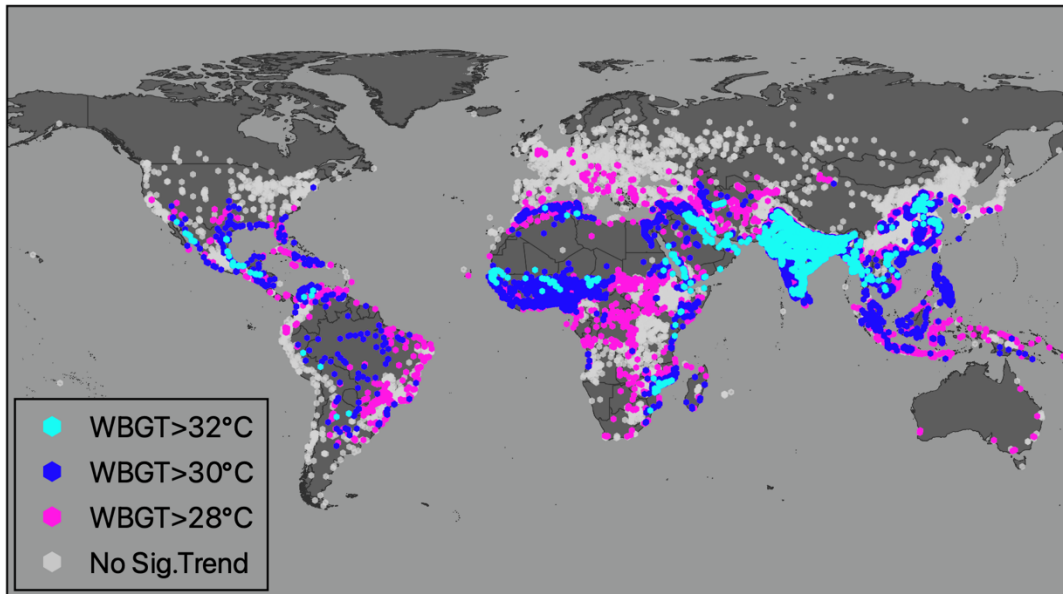


**Fig. S11** Urban settlements with a significant ( $p < 0.05$ ) increase in exposure from 1983 - 2016 for daily threshold of  $WBGT_{max} > 32^{\circ}C$  (2,979 urban settlements, turquoise),  $WBGT_{max} > 30^{\circ}C$  (5,985 urban settlements, blue),  $WBGT_{max} > 28^{\circ}C$  (7,628 urban settlements, pink), and no exposure trend measured at these thresholds (5,507 urban settlements, gray).

**Table S1:** Recently published global extreme heat studies. All studies use temperature input data that is coarser resolution than CHIRTS-daily (4) and those that use PGF or ERA5 likely underestimate extreme heat (4). The two studies (5, 6) that measure baseline population exposure do not delineate urban from rural exposure, nor assess how exposure trajectories have changed over time.

<b>Year Published</b>	<b>Heat Metric(s)</b>	<b>Population Exposure Baseline Measured?</b>	<b>Temperature Data</b>	<b>Spatial Resolution</b>	<b>Reference</b>
2021	3 day or longer periods where daily minimum air temperatures ( $T_{\min}$ ) > 99 <sup>th</sup> percentile of daily $T_{\min}$ over baseline (1985 - 2005)	Yes, global persons > 65 years old 1980 - 2020	ERA5	$0.5^{\circ} \times 0.5^{\circ}$	(5)
2020	Wet-bulb temperature > $35^{\circ}\text{C}$	No	HadISD	point data	(7)
2020	Variable - models heat-mortality relationship globally	No	PGF, BEST	administrative boundaries	(8)
2017	Plots daily maximum air temperatures ( $T_{\max}$ ) against relative humidity (RH) to identify mortality risk (person-days)	Yes, global total population ~2000	NCEP-DOE Reanalysis 2	$1.5^{\circ} \times 1.5^{\circ}$	(6)
2017	Wet-bulb temperature 30 - $35^{\circ}\text{C}$ (person-days)	No, projected exposure only	NCEP-DOE Reanalysis 2	$2^{\circ} \times 2^{\circ}$	(9)
2017	Heat index > $40.6^{\circ}\text{C}$ (person-days), standard wet bulb globe temperature > $35^{\circ}\text{C}$ SWBGT, and dry bulb > $37.6^{\circ}\text{C}$	No, only subset of 44 cities reported	ERA-Interim	$0.5^{\circ} \times 0.5^{\circ}$	(10)



2017	Apparent heat wave index, new percentile-based metric that combines temperature and humidity	No	ERA-Interim, Reanalysis 2	$1.875^\circ \times 1.875^\circ$	(11)
2016	Wet bulb globe temperatures (WBGT)	No, focuses on lost labor productivity	CRU	$0.5^\circ \times 0.5^\circ$	(12)

**Table S2.** Regions ranked by annual rate of increase in exposure from 1983 – 2016, with the percent of the global exposure trend, as well as percent contribution from total urban warming and urban population growth to the total exposure trajectories for each country using  $WBGT_{max} > 30^\circ C$ . See Materials and Methods for link to the entire dataset.

Rank	Region	Total Exposure (10 <sup>6</sup> people-days yr <sup>-1</sup> )	Pct. of Global Total	Pct. from Warming	Pct. from Population Growth
1	Southern Asia	1265.8	60%	35%	65%
2	Western Asia	299.9	14%	30%	70%
3	South-eastern Asia	173.5	8%	35%	65%
4	Sub-Saharan Africa	158.8	8%	30%	70%
5	Eastern Asia	124.6	6%	31%†	69%
6	Latin America and the Caribbean	41.6	2%	40%	60%
7	Northern Africa	35.8	2%	27%**	73%
8	Northern America	8.6**	0%	37%†	63%
9	Central Asia	0.1†	0%	-8%†	108%
10	Melanesia	0.1	0%	27%	73%
11	Australia and New Zealand	0.1†	0%	53%†	47%*
12	Eastern Europe	0†	0%	53%†	47%*
13	Northern Europe	0†	0%	83%†	17%†
14	Western Europe	0†	0%	74%†	26%†
15	Southern Europe	0†	0%	137%†	-37%†

All data points are significant at  $p < 0.001$ , unless otherwise indicated. \*\*  $p < 0.01$ , \*  $p < 0.05$ ,

† not significant.

**Table S3.** Top 25 countries worldwide ranked by annual rate of increase in exposure from 1983 – 2016, with the percent of the global exposure trend, as well as percent contribution from total urban warming and urban population growth to the total exposure trajectories for each country using  $WBGT_{max} > 30^{\circ}C$ . See Materials and Methods for link to the entire dataset.

Rank	Country	Total Exposure (10 <sup>6</sup> people-days yr <sup>-1</sup> )	Pct. of Global Total	Pct. from Warming	Pct. from Population Growth
1	India	1104	52.4%	38%	62%
2	Bangladesh	166.6	7.9%	37%	63%
3	Pakistan	143.1	6.8%	18%	82%
4	China	117.5	5.6%	28%†	72%
5	Nigeria	66	3.1%	39%	61%
6	Thailand	42.1	2%	25%**	75%
7	Vietnam	39.8	1.9%	33%	67%
8	Iraq	39.3	1.9%	38%	62%
9	Saudi Arabia	29.1	1.4%	19%	81%
10	United Arab Emirates	28.6	1.4%	3%	97%
11	Philippines	28.6	1.4%	32%**	68%
12	Myanmar	25.4	1.2%	46%	54%
13	Mexico	18.1	0.9%	34%	66%
14	Indonesia	17.5	0.8%	52%**	48%
15	Egypt	16.4	0.8%	53%	47%

16	Sudan	14.8	0.7%	-5%†	105%
17	Iran	13.1	0.6%	17%	83%
18	Chad	11.9	0.6%	18%**	82%
19	Senegal	10.8	0.5%	37%	63%
20	Yemen	10.3	0.5%	6%	94%
21	Singapore	10.1	0.5%	41%**	59%
22	Niger	9	0.4%	26%	74%
23	United States	8.6**	0.4%	37%†	63%
24	Venezuela	7.6	0.4%	39%	61%
25	Kuwait	7.5	0.4%	33%	67%

---

All data points are significant at  $p < 0.001$ , unless otherwise indicated. \*\*  $p < 0.01$ , \*  $p < 0/05$ ,  
† not significant.

**Table S4.** Top 50 urban settlements worldwide ranked by annual rate of increase in exposure from 1983 – 2016, with the percent of the global exposure trend, as well as percent contribution from total urban warming and urban population growth to the total exposure trajectories for each country using  $WBGT_{max} > 30^{\circ}C$ . See Materials and Methods for link to the entire dataset.

Rank	Urban Settlement	Country	Total Exposure (10 <sup>6</sup> people-days yr <sup>-1</sup> )	Pct. of Global Total	Pct. from Warming	Pct. from Population Growth
1	Dhaka	Bangladesh	57.5	2.7%	20%	80%
2	Delhi	India	55.4	2.6%	26%	74%
3	Kolkata	India	52.2	2.5%	52%	48%
4	Bangkok	Thailand	36.5	1.7%	18%	82%
5	Mumbai	India	29.3	1.4%	46%	54%
6	Karachi	Pakistan	26.6	1.3%	25%	75%
7	Chennai	India	26.1	1.2%	26%	74%
8	Dubai	United Arab Emirates	22.5	1.1%	2%	98%
9	Lahore	Pakistan	20.2	1%	9%†	91%
10	Manila	Philippines	18.3	0.9%	33%**	67%
11	Ahmadabad	India	17.3	0.8%	27%	73%
12	Guangzhou	China	15.3	0.7%	4%†	96%
13	Ho Chi Minh City	Vietnam	13.4	0.6%	21%**	79%
14	Shanghai	China	13.4	0.6%	16%†	84%

15	Lagos	Nigeria	13	0.6%	42%**	58%
16	Jiddah	Saudi Arabia	11.5	0.5%	11%**	89%
17	Comilla	Bangladesh	11.5	0.5%	45%	55%
18	Lucknow	India	11.3	0.5%	29%	71%
19	Yangon	Myanmar	11.2	0.5%	7%	93%
20	Singapore	Singapore	10.1	0.5%	41%**	59%
21	Baghdad	Iraq	9.9	0.5%	49%	51%
22	Benares	India	9.7	0.5%	31%	69%
23	Surat	India	9.6	0.5%	15%*	85%
24	Ha Noi	Vietnam	9.6	0.5%	13%**	87%
25	Patna	India	8.4	0.4%	26%	74%
26	Faisalabad	Pakistan	8	0.4%	11%**	89%
27	Shantou	China	7.7	0.4%	40%*	60%
28	Kanpur	India	7.6	0.4%	52%	48%
29	Kuwait City	Kuwait	7.2	0.3%	31%	69%
30	Asansol	India	7.1	0.3%	50%	50%
31	Multan	Pakistan	6.7	0.3%	15%	85%
32	Allahabad	India	6.6	0.3%	26%	74%
33	Cairo	Egypt	6.3	0.3%	54%	46%
34	Khartoum	Sudan	6.2	0.3%	7%†	93%
35	Agra	India	6.1	0.3%	27%	73%
36	Ar-Rayyan	Qatar	5.9	0.3%	5%	95%
37	Gujranwala	Pakistan	5.4	0.3%	10%*	90%
38	Hyderabad	Pakistan	5.4	0.3%	22%	78%
39	Suzhou, Jiangsu	China	5	0.2%	20%†	80%
40	Chittagong	Bangladesh	5	0.2%	46%	54%
41	Maracaibo	Venezuela	4.8	0.2%	38%	62%
42	Gorakhpur	India	4.8	0.2%	31%	69%
43	Ad-Dammam	Saudi Arabia	4.8	0.2%	20%	80%
44	Hyderabad	India	4.8	0.2%	50%	50%
45	Kousseri	Chad	4.5	0.2%	24%	76%
46	Manama	Bahrain	4.3	0.2%	12%	88%
47	Faizabad	India	4.2	0.2%	33%	67%

48	Mits'Iwa	Eritrea	4.1	0.2%	13%	87%
49	Tamluk	India	4.1	0.2%	40%	60%
50	Sirajganj	Bangladesh	4.1	0.2%	45%	55%

All data points are significant at  $p < 0.001$ , unless otherwise indicated. \*\*  $p < 0.01$ , \*  $p < 0/05$ , † not significant.

## SI References

1. G. Manoli, *et al.*, Magnitude of urban heat islands largely explained by climate and population. *Nature* **573**, 55–60 (2019).
2. UN-DESA, World Urbanization Prospects 2018 (2018) (August 30, 2018).
3. E. C. De Perez, *et al.*, Global predictability of temperature extremes. *Environ. Res. Lett.* **13**, 054017 (2018).
4. A. Verdin, *et al.*, Development and validation of the CHIRTS-daily quasi-global high-resolution daily temperature data set. *Sci Data* **7**, 303 (2020).
5. N. Watts, *et al.*, The 2020 report of The Lancet Countdown on health and climate change: responding to converging crises. *Lancet* **397**, 129–170 (2021).
6. C. Mora, *et al.*, Global risk of deadly heat. *Nat. Clim. Chang.* **7**, 501 (2017).
7. C. Raymond, T. Matthews, R. M. Horton, The emergence of heat and humidity too severe for human tolerance. *Science Advances* **6**, eaaw1838 (2020).
8. T. A. Carleton, *et al.*, Valuing the Global Mortality Consequences of Climate Change Accounting for Adaptation Costs and Benefits (2020) <https://doi.org/10.3386/w27599>.
9. E. Coffel, R. M. Horton, A. M. De Sherbinin, Temperature and humidity based projections of a rapid rise in global heat stress exposure during the 21st century (2017).
10. T. K. R. Matthews, R. L. Wilby, C. Murphy, Communicating the deadly consequences of global warming for human heat stress. *Proc. Natl. Acad. Sci. U. S. A.* **114**, 3861–3866 (2017).
11. S. Russo, J. Sillmann, A. Sterl, Humid heat waves at different warming levels. *Sci. Rep.* **7**, 7477 (2017).
12. T. Kjellstrom, Impact of Climate Conditions on Occupational Health and Related Economic Losses: A New Feature of Global and Urban Health in the Context of Climate Change. *Asia. Pac. J. Public Health* **28**, 28S–37S (2016).